N O T I C E

OCCURRENCE AND MINERAL CHEMISTRY OF HIGH PRESSURE PHASES,
PCTRILLO BASALT, SOUTHCENTRAL NEW MEXICO

Final

Technical Report

Principal Investigator: J. M. Hoffer
Period Covered: June 1, 1978 to May 31, 1980
Name of Institution: The University of Texas at El Paso

Grant Number: NASA NSG 9062

May 31, 1980

Department of
Geological Sciences

This Report

Represents an M.S. Thesis

by

Terri Smith Ortiz

Department of Geological Sciences

The University of Texas at El Paso

El Paso, Texas   79968

Thesis Director

Dr. J. M. Hoffer

ABSTRACT

Inclusions of clinopyroxenite, kaersutite-clinopyroxenite, kaersutite-rich inclusions, wehrlite and olivine-clinopyroxenite together with megacrysts of feldspar, augite, kaersutite and spinel are found loose on the flanks of cinder cones, as inclusions within lava flows and within the cores of volcanic bombs in the Quaternary alkali-olivine basalt of the West Potrillo Mountains, south-central New Mexico.

Based on petrological and geochemical evidence the megacrysts are interpreted to be phenocrysts which formed at great depth rather that xenocrysts of larger crystal aggregates. These large crystals are believed to have formed as stable phases at high temperature and pressure and have partially reacted with the basalt to produce subhedral to anhedral crystal boundaries.

It can be demonstrated that the mafic and ultramafic crystal aggregates were derived from an alkali-basalt source rock generated in the mantle. Thus, the inclusions are believed to represent a cumulus body or bodies injected within the lower crust or upper mantle. The crystal aggregate xenoliths exhibit varied mineralogies which stabilized at differing temperatures and pressures

TABLE OF CONTENTS

LIST OF FIGURES

LIST OF PLATES

LIST OF TABLES

INTRODUCTION

Location

The study area is located in the southern part of the West Potrillo Mountains, southwestern Dona Ana County, New Mexico, some 48 kilometers west of El Paso, Texas (Fig. 1). The area encompasses 384 square kilometers and is bounded on the south by the United States-Mexico border, on the east by longitude $107°07"W$, on the north by latidute $32°0"N$ and on the west by longitude $107°15"W$.

The area is easily accessible by traveling north on Interstate 10 from El Paso to the Mesa Street Exit then traveling west on Mesa Street to Country Club Road. Turn right on McNutt Road and travel west onto the La Mesa surface 4.8 kilometers (across the railroad tracks) and bear right through Strauss, New Mexico. Turn left at the Columbus Road to Mt. Riley and Columbus, New Mexico. Travel west for about 32 kilometers approximately paralleling the international border. Access to the study area is from ranch roads north of the Columbus Road.

Purpose

The purpose of this investigation was to systematically collect and analyze the megacrysts and xenoliths found within the West Potrillo Basalt, Dona Ana County,

1
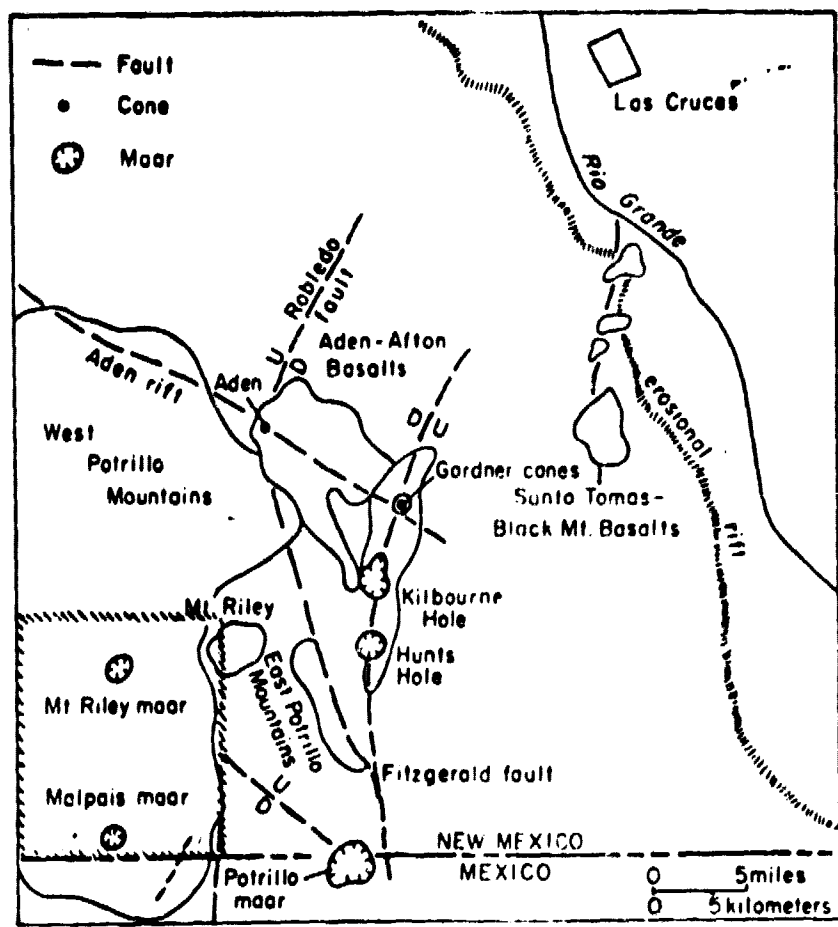
Fig. 1. Index map of the Potrillo Basalt Field, study area shown in hatchers (after Hoffer, 1976).

New Mexico. To date, the only detailed mineralogic work on the xenoliths has been on the feldspar megacrysts reported by Hoffer and Hoffer (1973).

The present investigation involved a detailed petrological and geochemical investigation of all types of inclusions present in the West Potrillo Basalt. In this paper megacrysts are defined as single crystals exceeding 3 millimeters in length. Crystal aggregate xenoliths are foreign rock fragments composed of more than two types of minerals. Inclusions refer to both megacrysts and crystal aggregate xenoliths that are associated with the West Potrillo Basalt. The main areas of focus encompassed analyses to determine the source and depth of origin of the megacrysts and xenoliths and determination of the relationship of the two groups.

Previous Work

Renault (1970) first analyzed and reported the major element geochemistry of the West Potrillo Basalts while Hoffer (1976) discussed the regional geology and the petrology of the basalt and the geochemistry of the basalt in relation to the Rio Grande rift. Malpai Maar, a maar volcano, is located in the south-central portion of the study area and was studied in detail by Page (1973).

Considerable work has been published on the xenoliths of Kilbourne Hole, a maar volcano located east of the

study area (Fig. 1). The results of these studies are included in reports by Carter (1970), Padovani and Carter (1977), Reid (1978), Padovani (1978) and Grew (1979).

Physiography

The Potrillo basalt flows were erupted onto the La Mesa surface, a flat plain developed within the Mesilla Bolson during middle to late Pleistocene (Hawley and Kottlowski, 1969). The major portion of the Potrillo Basalt, the West Potrillo Basalt, forms a broad, north-trending constructional plateau. The area is included in the Mexican highland section of the Basin and Range province (Fenneman, 1931).

Geologic Setting

Regional Geology

The West Potrillo Mountains are located in the southern Rio Grande rift (Fig. 2). Rifting began in the southern portion of the rift approximately 32 million years before present with abundant volcanic activity between 32-29 million years ago and again at 13 million years ago (Chapin, 1978). A sharp acceleration in basaltic volcanism occurred beginning 5 million years ago including the basalts of the West Potrillo Mountains. According to the rift model of Salvenson (1978), volcanism in the study area is the direct result of rifting.
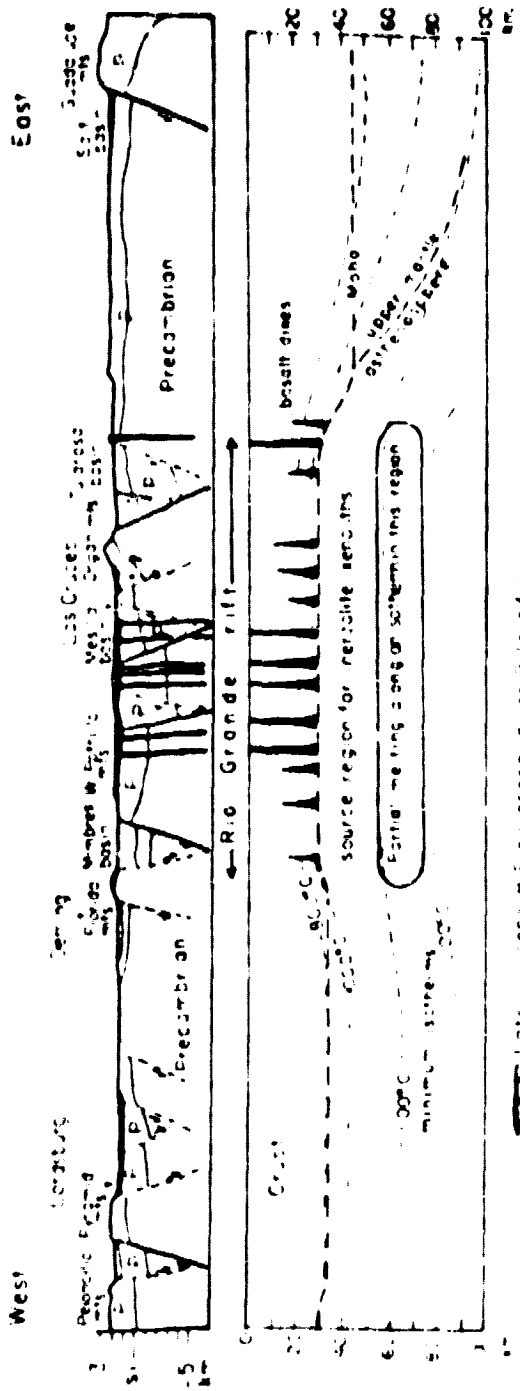
Fig. 2. Interpretive cross-section of the crust and upper mantle across the southern Rio Grande rift along latitude 32°N. Section is based on gravity, seismic, heat flow and conductivity data (after Seager and Morgan, 1979).

Rifting apparently continues at the present time as evidenced by fault scarps cutting Pleistocene deposits, high heat flow, recent changes in elevation, detection of magma bodies and geophysical evidence for anamalous crust and upper mantle beneath the rift (Chapin, 1978).

Hoffer (1976) states that the chemistry of the West Pot illo Basalt is typical of the volcanic rock types which occur along the flanks of the Rio Grande rift to the north. A hypothetical cross section 100 kilometers in depth constructed for the region just north of the study area is shown in Fig. 2. The Rio Grande rift provided an environment of volcanism which brought the inclusions of the West Potrillo Basalt to the surface.

Other geologic structures in the area include the Mt. Riley-Mt. Cox intrusion, a light-colorea, microporphyritic andesite to rhyodacite which is located just to the eas of the study area (Millican, 1971; see Fig. 1) and the East Potrillo Mountains which are also to the east of the study area and are composed of Permian and Cretaceous sedimentary rocks which are deformed by north-trending faults (Bowers, 1960, see Fig. 1). West of the study area are scattered outcrops of Permian and Cretaceous sedimentary rocks and Tertiary volcanic and intrusive rocks.

The West Potrillo Basalt

The term Potrillo Basalt refers to the Quaternary basaltic lava flows and associated cones that crop out between the Rio Grande valley and the Mimbres valley including the rocks of the West Potrillo Mountains, Santo Tomas-Black Mountain area and the Aden Crater-Kilbourne Hole region (Hoffer, 1976). Three separate periods of volcanic activity have been distinquished. From oldest to youngest they are: the West Potrillo Basalt, Afton Basalt and Aden Basalt (Hoffer, 1976). The West Potrillo Basalt is an olivine basalt extruded 140,000 to 200,000 years before present and contains both the megacrysts and xenoliths which are the topic of this study. Lack of erosion prevents determination of the thickness of the lava pile, but a well located 8 kilometers south of Mt. Riley (see Fig. 1) penetrated 85.5 meters of lava interbedded with sand and gravel (King and others, 1969). The flows average 5.1 meters in thickness.

The basalt is vesicular and variable in color from dark gray to black to blue-black to reddish brown depending on the flow, chemistry, weathering and reaction of the melt with gases during eruption of individual flow units. Hoffer (1976) has described the basalt as hypocrystalline with microphenocrysts consisting of olivine, plagioclase and pyroxene. The groundmass is microcrystalline with intersertal to intergranular texture and is composed of

pyroxene and plagioclase with minor amounts of opaques, olivine and glass.

The basalt of the West Potrillo Mountains is classified as alkaline-olivine basalt on the basis of the ratio of total alkali to silica. The average analysis shows low SiO_2 (44.54 percent), moderate Al_2O_3 (15.40 percent), high total alkali (Na_2O plus K_2O equals 4.96 percent) and moderately high TiO_2 (2.29 percent) (Hoffer, 1976; see Table 1).

Based on petrography and chemistry, Hoffer (1976) divides the West Potrillo Basalt into two members. Member 1 is an older plagioclase-rich, olivine-poor basalt with minor mafic and ultramafic xenoliths while Member 2 is a younger olivine-rich basalt with higher MgO content containing relatively abundant mafic and ultramafic xenoliths. Hoffer (1976) suggests that the difference in composition between the two members of the unit is a result of eruption from a magma chamber in which crystal settling had occurred.

Cinder Cones

Cinder cones are very abundant in the West Potrillo Mountains. Over 150 cones have been mapped. Typically, the cones are composed of basal agglutinated cinder, bedded cinder, bombs and a partial to complete spatter rim at the top. Most are horseshoe-shaped in plan

TABLE 1

CHEMICAL ANALYSES OF WEST POTRILLO BASALT

Chemical Analyses of West Potrillo Basalt (POT samples by J. Renault, 1970, New Mexico Bureau of Mines and Mineral Resources; WP samples by T. Asari, Japan Analytical Laboratory; analyses after Hoffer, 1976).

SAMPLE	MEMBER 1			MEMBER 2		
	WP-1	WP-2	POT19	WP-3	POT22	POT16
SiO_2	44.63	44.37	45.16	44.21	44.42	45.48
TiO_2	2.60	2.37	2.20	2.21	2.34	2.23
Al_2O_3	15.92	15.98	15.07	15.01	15.44	16.22
Fe_2O_3	3.66	4.13		4.82		
FeO	6.56	6.82	*9.95	6.07	*9.93	*9.45
MnO	0.14	0.16	0.19	0.14	0.18	0.17
MgO	9.17	7.30	8.97	10.34	10.92	10.17
CaO	10.36	10.09	9.84	10.94	10.72	9.66
Na_2O	4.70	4.48	3.40	3.67	3.38	3.60
K_2O	0.90	2.27	1.74	1.65	1.54	1.44
H_2O	1.60	1.90	nd	nd	nd	nd
P_2O_5	0.64	0.74	nd	nd	nd	nd
TOTAL	100.88	100.61	97.12	99.54	98.87	98.42

*Represents Total Fe Reported as FeO; nd represents not determined.

view, with one or more vents. Cinder cones vary from 60 to 150 meters in height and from 300 to 900 meters in diameter (Hoffer, 1976, see Plate 1).

Hoffer (1976) divides the cones into two age groups based on shape and degree of dissection. The younger cones are generally large and steep-sided with slopes from 20-25 degrees. Most are relatively undissect- ed by erosion with their slopes possessing shallow, closely-spaced arroyos. These cones usually contain a single vent with a breached rim through which a lava flow had been extruded.

The older cones display a more subdued shape with slopes of 10-20 degrees. Deep arroyos cut the slopes and in addition occur in complexes with multiple vents ar- ranged in irregular to linear patterns. Those with linear patterns trend north.

No correlation between age of cones and inclusion occurrence has been noted during systematic sampling of the xenoliths. Megacrysts and xenoliths are found associated with approximately 85 percent of the cones although the inclusions are much more abundant in certain areas and particular types of inclusions are locally concentrated.

The basalt in the study area is essentially unde- formed although two faults have been noted in the southeast part of the study area. Fault 1 is a north- trending probable fault mapped by Hoffer (1976) inferred
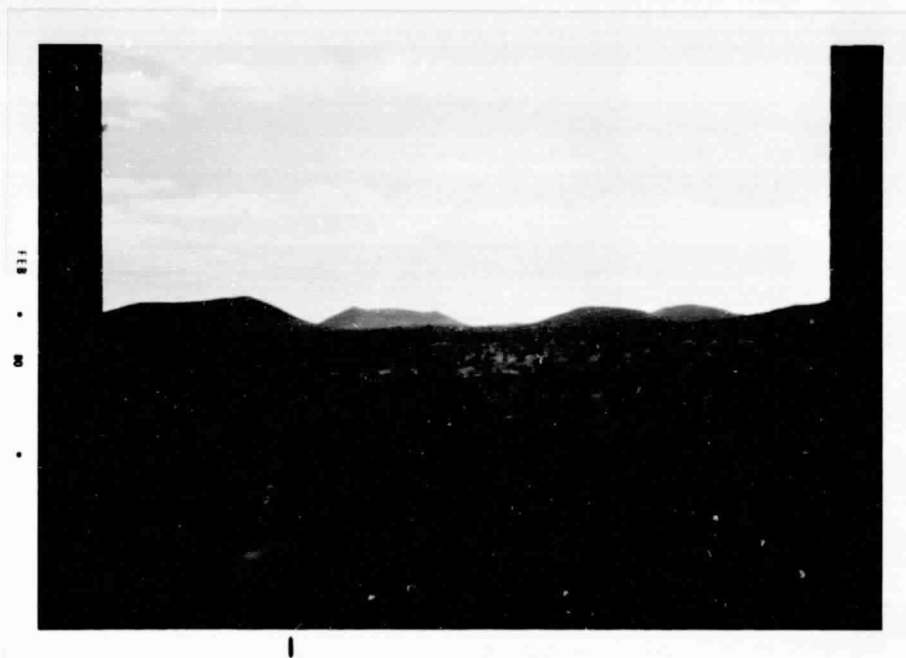
Plate 1. View of Quaternary cinder cones of the West Potrillo Basalt in study area looking northwest. Scale: brush in foreground is one meter high.

from a prominent 18 meter high west-facing scarp of caliche-cemented alluvium. Fault 1 is a lineament about two to three kilometers west of Fault 1 noted by Bersch (1977) from aerial photographs (see Fig. 3).

Methods of Analysis

Collection of Samples

Sampling of mafic and ultramafic crystal aggregate xenoliths as well as megacrysts was completed during the summer and fall of 1978. Inclusions and megacrysts were collected on and around individual cinder cones in the West Potrillo Mountains (Fig. 3; Apprendix A). An attempt was made to select samples that were representative in size, abundance, and composition. A total of 1316 samples were collected and cataloged. Of this total, 697 were feldspar megacrysts, 169 were predominantly pyroxene and 450 contained easily recognizable amphibole.

Preparation of Samples

Samples were then prepared for various types of analyses including thin section, X-ray flourescence, gamma spectrometry, X-ray diffraction and scanning electron microscopy carried out during the spring and summer of 1979.

First, rocks and megacrysts were selected for thin section analysis. Twenty-five thin sections were prepared

at the University of Texas at El Paso and one hundred and twelve thin sections were prepared by a commercial thin section laboratory.

Selected samples including five feldspar mega-crysts and eight mafic and ultramafic xenoliths were chem-ically analysed by the National Aeronautics and Space Administration laboratory in Houston, Texas using X-ray fluorescence. Individual analyses were repeated four times.

In addition, two amphibole megacrysts, one amphi-bole crystal aggregate (98 percent amphibole), one pyrox-ene crystal aggregate and one pyroxene megacryst as well as twenty-eight feldspars were ground in a disc grinder, filtered to minus 500 mesh and pellitized for chemical analysis on an Ortec TEFA Model 6110 X-ray energy disper-sive fluourescence analyzer.

Next, fourteen samples including two feldspar megacrysts, one amphibole megacryst, two basalt samples and nine mafic and ultramafic crystal aggregates were ground in a disc grinder and filtered to minus 35 mesh. The samples were then weighed and sealed in containers and allowed to reach equilibrium for over three weeks pri-or to counting on a nuclear data pulse analyzer.

Forty-two samples were selected for X-ray dif-fraction analysis. These samples were initially ground and then filtered to minus 200 mesh. Samples selected

included twenty-eight feldspar megacrysts, two amphibole megacrysts, one amphibole crystal aggregate (98 percent amphibole), one pyroxene megacryst, one spinel megacryst and ten mafic and ultramafic crystal aggregate xenoliths.

Finally, seven feldspar megacrysts and six mafic and ultramafic aggregates were prepared and coated with carbon for analysis on a Materials Analysis Corp. scanning electron microscope connected to an EDAX analyzing unit.

FELDSPAR MEGACRYSTS

Occurrence

Feldspar megacrysts are the most abundant type of inclusion in the West Potrillo Basalt (see Appendix A). Alkali feldspar and plagioclase megacrysts (single crystals) exceeding three millimeters in length are found as loose crystal on the flanks of cinder cones, in the cores of volcanic bombs, and as inclusions in lava flows. The size and abundance of the crystals varies from location to location. Feldspar crystals occur throughout the area but are most abundant in the north-central and west-central portions of the study area.

Petrography

The feldspar crystals are typically anhedral to euhedral, grey to colorless and range in size from three millimeters to six centimeters (Plate 2 and Plate 3). Iron oxide staining commonly coats the crystals various shades of red and red brown. Twinning lamellae are often visible in the plagioclase crystals, and conchoidal fracture is also common. The megacrysts are commonly iridescent indicating the feldspars are of peristerite composition (An3-An22). Albite twinning is common in the crystals although twinning is absent in some. Albite

15

Plate 2. Representative samples of feldspar megacrysts of the West Potrillo Basalt. Note dime for scale.
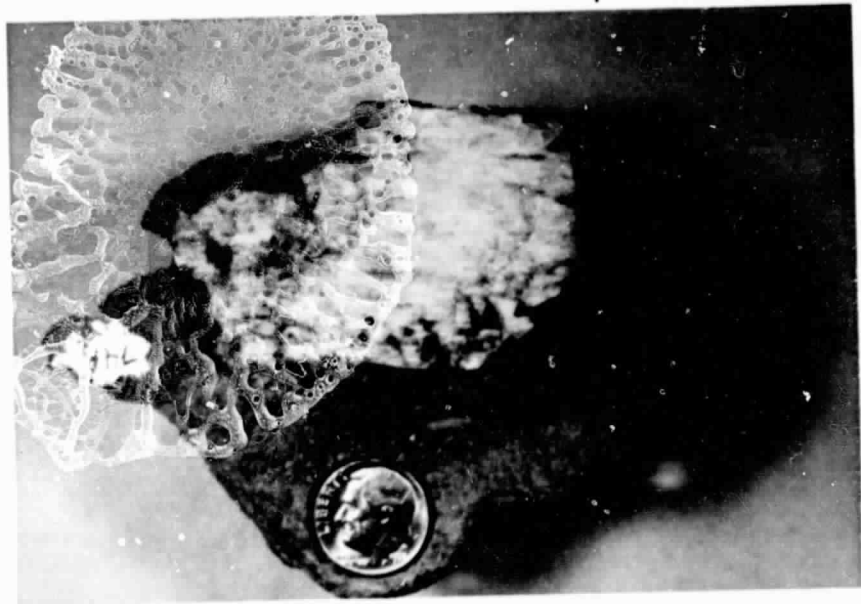
Plate 3. Large feldspar megacryst included in basalt from the West Potrillo Basalt.

twinning and pericline twinning occur together in only two crystals.

The megacrysts show varying intensities of strain shadows possibly developed at depth or perhaps due to unloading at the surface (Plate 4). Microfaults (Plate 5) are present in a small percent of the megacrysts and one crystal shows very slightly bent twin lamellae indicating deformation at near liquidus temperature (Plate 6).

Inclusions of iron oxide and apatite are present in some of the megacrysts. No zoning is noted either in thin section or on the scanning electron microscope. Little to no reaction has taken place between the included crystals and the host basalt other than rounding and slight corrosion of crystal edges. A brief description of feldspar megacrysts collected is compiled in Appendix B.

Chemistry

Analysis was carried out on five selected samples using X-ray fluorescence at NASA and the results of the analyses are presented ir Table 2. It is noteworthy that the results do not total 100 percent, but range from 96.96 percent to 98.02 percent, leaving 2-3 percent unaccountable. A qualitative X-ray scan of each sample revealed the presence of no major or minor elements other than those reported.

Twenty eight feldspars were analysed at the
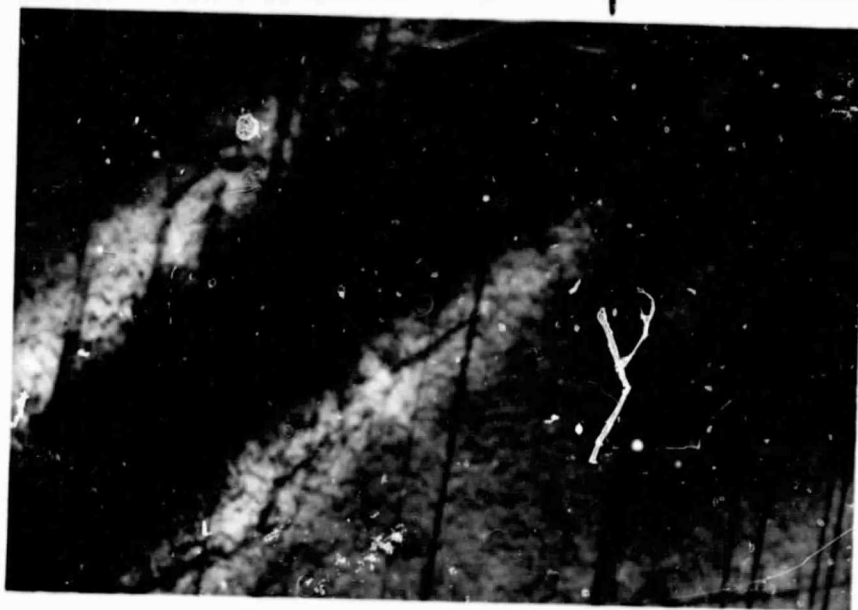
Plate 4. Strain shadows in plagioclase
megacryst observed under petrographic micro-
scope using crossed nicols. Magnification 20X.

Plate 5. Microfaults in plagioclase megacryst observed under petrographic microscope using crossed nicols. Magnification 20X.
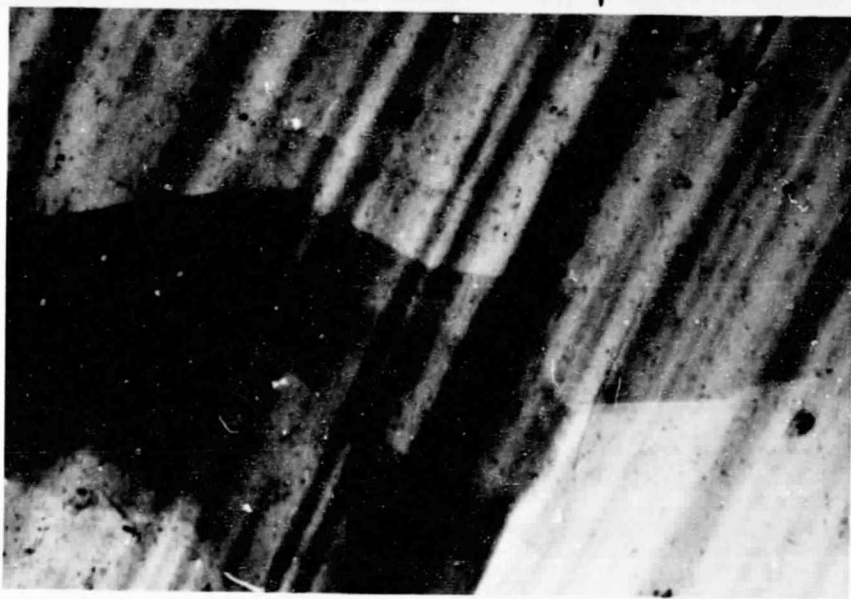
Plate 6. Slightly bent twin lamellae in
plagioclase of the West Potrillo Basalt as
observd under petrographic microscope using
crossed nicols. Magnification 20X.

TABLE 2

CHEMICAL ANALYSES OF FELDSPAR MEGACRYSTS, WEST POTRILLO BASALT

Samples Analyzed at the National Aeronautics and Space Administration Laboratory, Houston, Texas, using X-ray fluorescence.

SAMPLE	13	62	66	72	221
SiO_2	62.67	62.13	63.47	63.74	61.99
TiO_2	0.02	0.02	0.02	0.03	0.02
Al_2O_3	21.96	22.96	21.38	20.84	21.41
Fe_2O_3	0.27	0.22	0.20	0.28	0.27
FeO	0.00	0.00	0.00	0.00	0.00
MnO	0.00	0.00	0.00	0.00	0.00
MgO	0.12	0.09	0.08	0.12	0.14
CaO	2.86	3.86	2.21	1.86	2.67
Na_2O	6.70	6.57	6.85	6.45	6.71
K_2O	2.84	1.80	3.18	3.88	3.22
P_2O_5	0.03	0.00	0.01	0.06	0.03
S	0.00	0.00	0.00	0.00	0.00
Total H_2O	0.32	0.37	0.29	0.36	0.51
TOTAL	97.79	98.02	97.69	97.54	96.96

University of Texas at El Paso (Table 3). Totals range
from 98.18 percent to 101.60 percent. Although many ana-
lyses appear good, calculation of the normative Or, Ab and
An totals ranged from only 83.1 up to 101.9 with only 4
calculations within 2 percentage points of 100. The pres-
ence of barium was checked by atomic absorption but was
negligible. The low totals may indicate low determined
values of the alkali elements.

Two feldspar crystals were analysed by gamma spec-
trometry. The first was found to contain 2.52 percent
potassium, 1.51 parts per million uranium and 1.87 parts
per million thorium. The second contained 2.52 percent
potassium, 0.47 parts per million uranium and 1.90 parts
per million thorium.

Classification

The feldspar megacrysts were classified on the
basis of chemical anlayses. X-ray diffraction data and
petrographic analyses are in agreement with the classifi-
cation. Figure 4 shows the composition of the feldspar
megacrysts in which the end members Or, Ab, and An were
calculated from the chemical analyses and plotted on a
standard Or-Ab-An triangle. The majority of the mega-
crysts fall in the fields of lime anorthoclase and potash
oligocalse although anorthoclase, andesine and potash
andesine are also represented. The megacrysts appear to

TABLE 3

	Anorthoclase	Andesine	Andesine	Oligoclase	Potash Oligoclase	Oligoclase	Anorthoclase

CHEMICAL ANALYSES OF FELDSPAR MEGACRYSTS, WEST POTRILLO BASALT

Samples analyzed at the University of Texas at El Paso using Ortec TEFA model 6110 X-ray energy dispersive fluorescence analyzer.

Sample	13K	621K	621H	75F	67J	68L	57K
SiO_2	65.59	60.47	60.74	61.40	58.07	62.33	64.61
TiO_2	0.02	0.02	0.03	0.04	0.04	0.04	0.03
Al_2O_3	20.68	24.92	24.84	23.74	27.15	23.35	21.29
Fe_2O_3	0.25	0.37	0.33	0.34	0.39	0.28	0.26
MnO	0.00	0.00	0.00	0.00	0.00	0.00	0.00
MgO	0.14	0.12	0.15	0.10	0.12	0.12	0.07
CaO	0.86	5.44	5.36	4.27	8.30	3.91	1.69
Na_2O	8.62	8.00	7.97	8.59	5.89	8.38	8.56
K_2O	4.84	1.08	1.20	1.23	1.06	1.49	3.13
Total	101.00	100.42	100.62	99.71	101.02	99.90	99.64
Or%	26.0	6.0	6.7	6.9	6.2	8.5	17.9
Ab%	70.1	68.3	68.0	73.0	52.6	72.7	74.0
An%	3.9	25.7	25.3	20.1	41.1	18.8	8.1
Total	100.0	100.0	100.0	100.0	99.9	100.0	100.0

TABLE 3

Continued

Sample	Andesine	Anorthoclase	Andesine	Anorthoclase	Potash Oligoclase	Potash Oligoclase	Anorthoclase
	13L	54M	551A	56K	61K	621I	621J
SiO_2	60.34	64.44	59.57	64.87	63.54	63.05	64.28
TiO_2	0.04	0.03	0.04	0.03	0.04	0.02	0.01
Al_2O_3	24.83	21.29	25.65	21.31	22.49	22.47	21.54
Fe_2O_3	0.39	0.26	0.34	0.22	0.25	0.29	0.23
MnO	0.00	0.00	0.00	0.00	0.00	0.00	0.00
MgO	0.11	0.10	0.12	0.11	0.11	0.10	0.09
CaO	5.56	1.60	6.61	1.53	2.86	2.78	1.91
Na_2O	6.63	7.85	6.10	7.75	8.39	8.82	8.68
K_2O	1.08	3.66	1.22	3.32	1.88	2.14	3.18
Total	98.98	99.23	99.62	99.14	99.56	99.67	99.92
Or%	6.8	21.6	7.6	20.3	11.1	12.0	17.7
Ab%	63.6	70.4	57.8	71.8	74.8	75.0	73.3
An%	29.5	8.0	34.6	7.9	14.1	13.0	9.0
Total	99.9	100.0	100.0	100.0	100.0	100.0	100.0

TABLE 3

Continued

Sample	Potash Oligoclase 621L	Anorthoclase 63S	Oligoclase 63T	Oligoclase 64M	Anorthoclase 64N	Anorthoclase 64Q	Anorthoclase 66-0
SiO_2	63.19	63.18	60.26	60.68	64.80	63.00	64.25
TiO_2	0.73	0.01	0.03	0.03	0.03	0.02	0.02
Al_2O_3	22.56	21.64	24.18	24.61	21.21	21.45	21.43
Fe_2O_3	0.32	0.34	0.42	0.38	0.19	0.66	0.27
MnO	0.00	0.00	0.00	0.00	0.00	0.00	0.00
MgO	0.12	0.09	0.12	0.09	0.11	0.10	0.13
CaO	2.73	1.80	5.19	5.18	1.65	1.38	1.77
Na_2O	8.08	8.87	9.06	8.54	8.42	9.37	9.27
K_2O	2.17	3.13	1.17	1.11	3.43	3.16	3.48
Total	99.90	99.06	100.43	100.62	99.84	99.14	100.62
Or%	13.0	17.3	6.1	6.0	19.5	17.0	18.3
Ab%	73.3	74.4	71.3	70.4	72.6	76.7	73.9
An%	13.7	8.3	22.6	23.6	7.9	6.3	7.8
Total	100.0	100.0	100.0	100.0	100.0	100.0	100.0

TABLE 3

Continued

	Oligoclase	Oligoclase	Anorthoclase	Potash Oligoclase	Anorthoclase	Anorthoclase	Potash Oligoclase
Sample	67C	68F	751E	751P	76B	13C	57A
SiO_2	60.29	61.33	63.88	63.28	64.68	64.44	61.48
TiO_2	0.04	0.03	0.02	0.03	0.02	0.03	0.03
Al_2O_3	24.95	24.32	21.88	22.81	21.48	21.14	24.44
Fe_2O_3	0.39	0.36	0.36	0.28	0.27	0.16	0.18
MnO	0.00	0.00	0.00	0.00	0.00	0.00	0.00
MgO	0.14	0.11	0.12	0.11	0.07	0.11	0.15
CaO	5.37	4.57	1.86	3.12	1.65	2.02	5.30
Na 0	7.83	7.42	8.60	8.35	9.36	8.65	7.30
K_2O	1.29	1.21	3.40	1.73	2.99	3.87	1.40
Total	100.30	99.35	100.12	99.71	100.52	100.42	100.28
Or%	7.3	7.4	18.9	10.2	16.1	20.7	8.3
Ab%	67.2	69.0	72.4	74.4	76.4	70.2	65.4
An%	25.5	23.5	8.7	15.4	7.5	9.1	26.3
Total	100.0	99.9	100.0	100.0	100.0	100.0	100.0
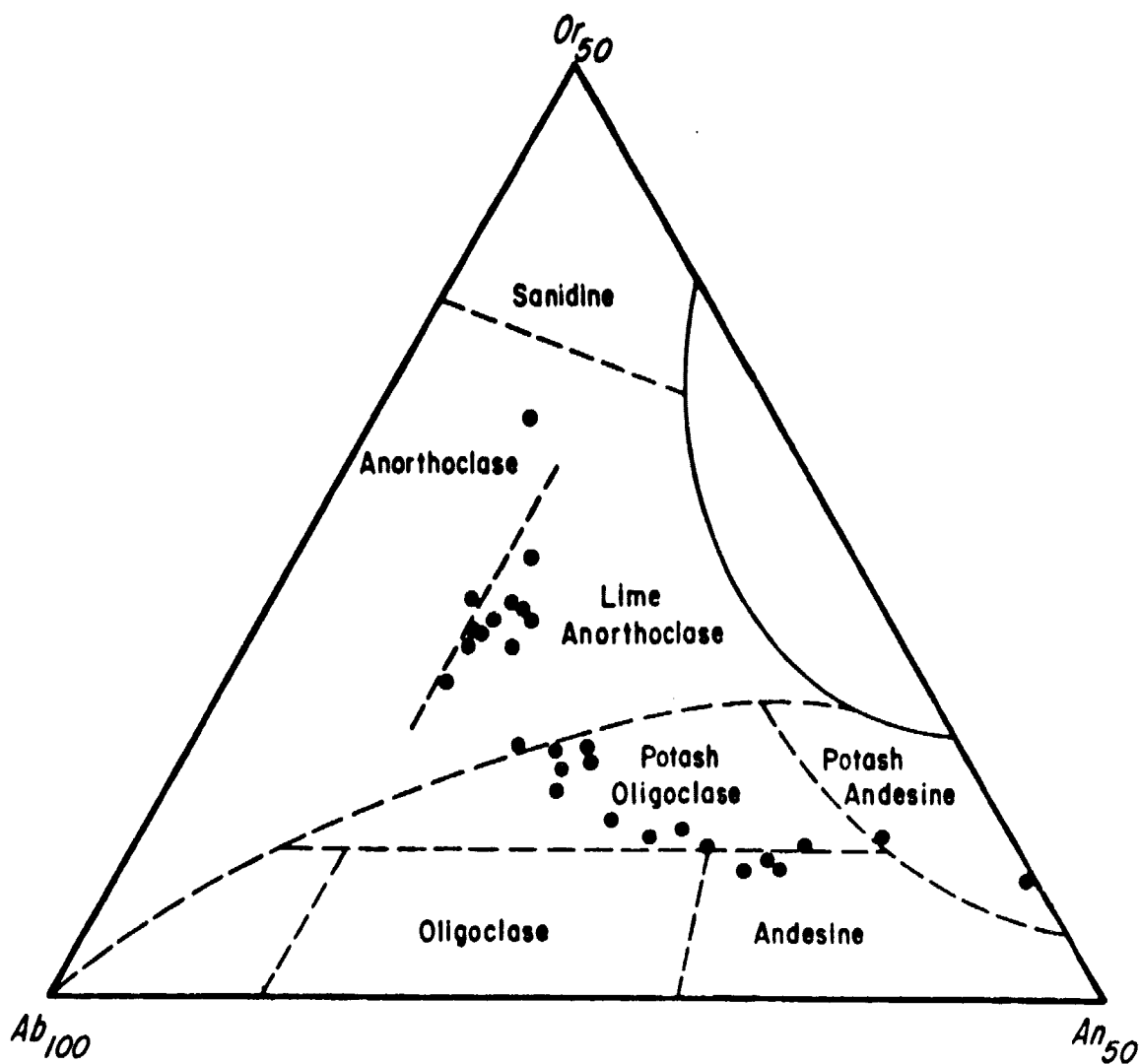
Fig. 4. Molecular composition of feldspar
megacrysts in West Potrillo Basalt, New Mexico
as analysed by Hoffer at the University of
Texas at El Paso and recaluted to Or, Ab and
An content. Based on classification of Muir
(1961) where Or is $KAlSi_3O_8$, Ab is $NaAlSi_3O_8$,
and An is $CaAl_2Si_2O_8$.

fall along a trend extending from potash andesine to lime anorthoclase or in a cluster of points in the Or-20, Ab-70, An-10 portion of the diagram with a trend from potash oligoclase to potash andesine. Different compositions of feldspar do occur in the same spatial area in the West Potrillo Basalt as shown in Table 3. For example, samples 621H, 621I, 621J, 621K and 621L were all collected only a few feet apart but differ significantly in composition.

MAFIC AND ULTRAMAFIC INCLUSIONS

Occurrence

Mafic and ultramafic crystal aggregate xenoliths and megacrysts occur much in the same way as the feldspar megacrysts. Again, the most common occurrence is as loose crystals on the flanks of cinder cones. The inclusions are also found included in basalt and as cores of volcanic bombs. Crystal aggregate xenoliths include clinopyroxenites, wehrlite and kaersutite-rich inclusions. The xenoliths are typically three centimeters in diameter or smaller (Plate 7 and Plate 8) however, a sample thirty centimeters in length has been collected. The basic aggregates are common throughout the West Potrillo Mountains, but especially in the southwestern part of the study area.

Megacrysts of kaersutite, augite and spinel are also found in the area (see Plate 9). Kaersutite is the most abundant of the three types and crystals range in size from a few millimeters up to six centimeters. Some fragments apparently represent cleavage fragments. Augite megacrysts are difficult to distinquish from the amphibole in hand sample since both tend to have rounded shapes and often a dull appearance. Augite megacrysts range in size from one to four centimeters. Spinel megacrysts have a dull, tar-like appearance and average one centimeter in

30

Plate 7. Representative ultramafic crystal
aggregate xenoliths of the West Potrillo
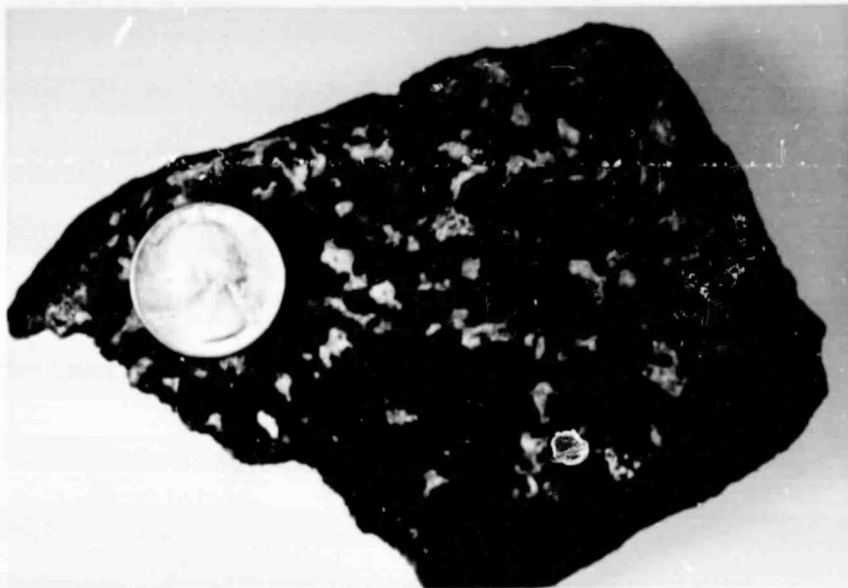Basalt. Note weathered appearance. Dime for
scale.

Plate 8. Large mafic xenolith with an un-
usually high percent feldspar, West Potrillo
Basalt, New Mexico. Kaersutite and augite
also present. Quarter for scale.

Plate 9. Ultramafic megacrysts of West
Potrillo Basalt, New Mexico. Augite upper
righthand corner; spinel upper lefthand
corner; and the remaining consist of kaersu-
tite. Dime for scale.

size. Again, the megacrysts of kaersutite, augite and
spinel are most abundant in the north-central and west-
central parts of the study area.

Textures of Crystal Aggregate Xenoliths

Mafic and ultramafic crystal aggregate xenoliths
typically hav encmorphic granular or polygonal textures
which are neither clearly igneous or metamorphic. Because
of the small size of the crystal aggregates, which average
2.5 centimeters in diameter relative to the large size of
individual grains (one to five millimeters) and because it
is difficult to be certain of spatial relationships it is
difficult to ascertain the origin of the inclusions.

A number of writers have defined the textural
terms used to describe cumulus rocks, but those of Wager,
Brown and Wadsworth (1960) are the most widely accepted.
There are two stages in the formation of cumulus rocks: 1)
the accumulation of the precipitated cumulus crystals, and
2) the filling of the intercumulus space. The final tex-
ture of a cumulus rock is largely the result of the second
process. The intercumulus interstices can be filled by
two processes 1) continued growth of the cumulus crystals,
referred to as adcumulus growth, or 2) crystallization of
one or more new intercumulus minerals from the intercu-
mulus liquid.

An adcumulate is defined as a cumulus rock in

which most or all of the intercumulus space has been filled by the adcumulus growth of the cumulus crystals. Adcumulus textures tend to be equigranular with polygonally interlocking grains. An orthocumulate is defined as a cumulus rock in which the cumulus crystals have undergone little or no adcumulus growth, and the intercumulus texture is filled mainly with new phases.

Intercumulus phases of amphibole and feldspar are present in some samples (see Plate 10 and Plate 11), and thus are termed orthocumulates. Adcumulates are much more common (see Plate 13). In many cases, however, polyphase aggregates do not display obvious cumulus characteristics because, as noted by Wager and others (1960), if three or four phases are cumulus, subsequent crystallizaion of the intercumulus liquid will simply enlarge the cumulus grains, resulting in "ordinary" igneous texture.

Small inclusion size limits recognition of layers of contrasting mineral composition, also common in cumulus rocks. However, as observed occasionally in thin section, black spinel is locally abundant and virtually absent over the remainder of the slide. One unusually large xenolith does display alternating layers typical of cumulus texture (Plate 12). Mineral relations are for the most part consistant with those associated with cumulus processes and therefore these rocks are believed to be cumulates.

The reaction between inclusions and the basalt
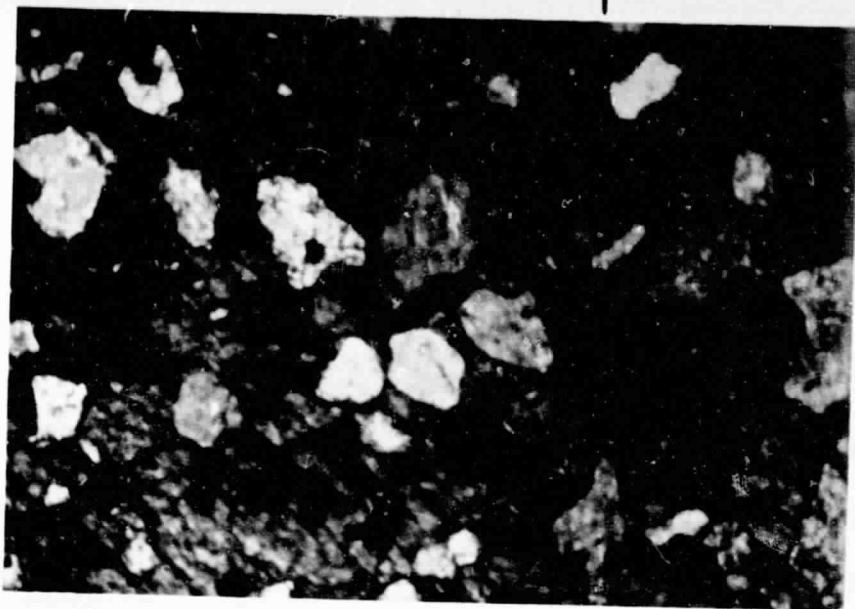
Plate 10. Intercumulus keersutite forming
poikilitic texture in ultramafic inclusion of the
West Potrillo Basalt as observed under crossed
nicols. Included grains are spinel, olivine
and pyroxene. Magnification: 20X.
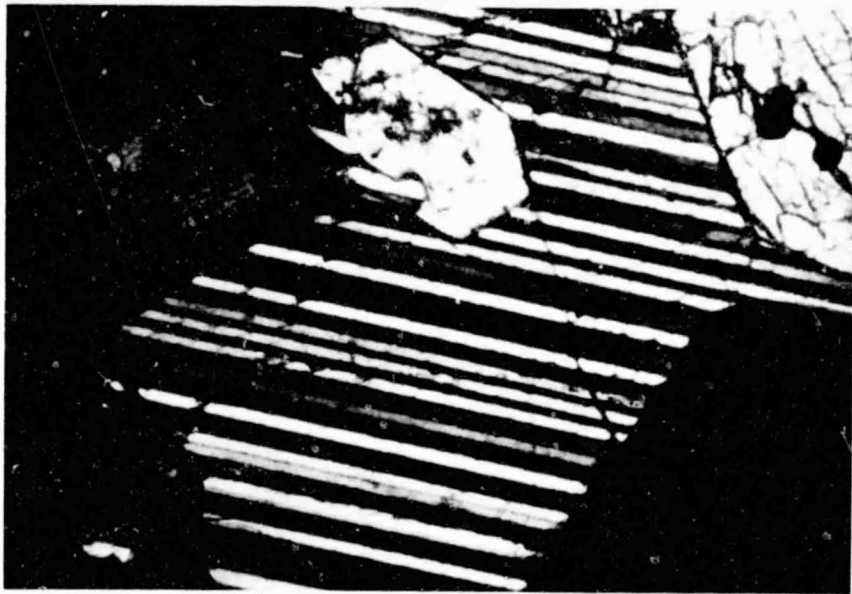
Plate 11. Intercumulus feldspar within ultra-
mafic xenolith of the West Potrillo Basalt as
observed under crossed nicols. Magnifica-
tion: 20X.
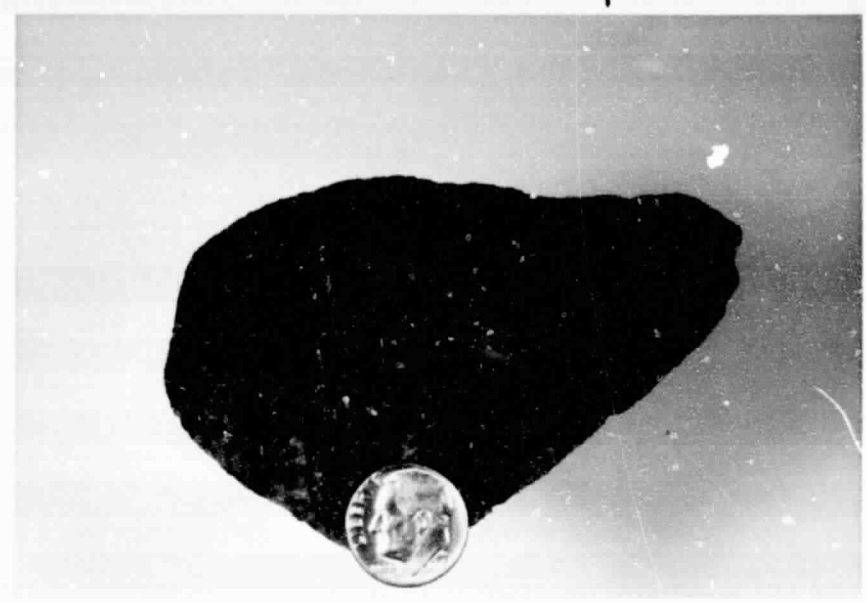
Plate 12. Alternating cumulus layers in un-
usually large xenolith of the West Potrillo
Basalt. Dime for scale.
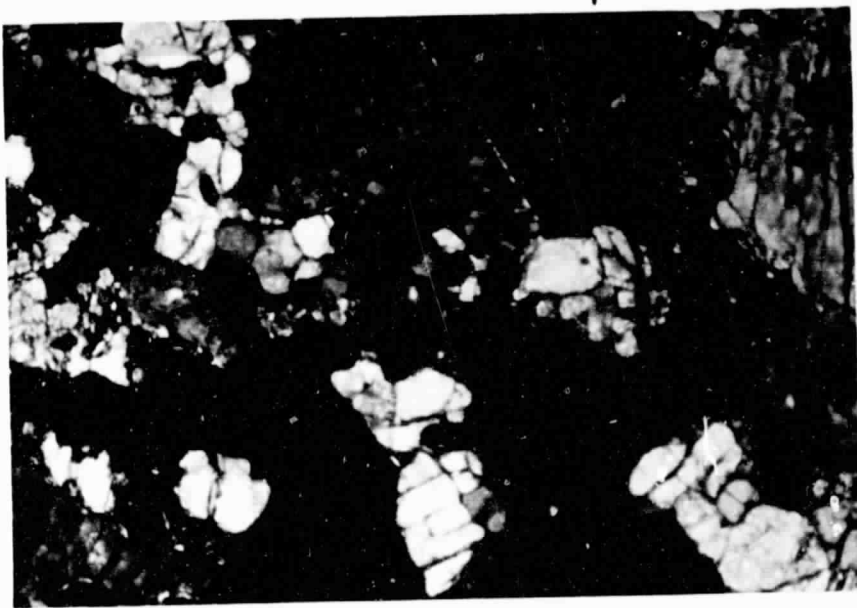
Plate 13. Typical texture of ultramafic crystal
aggregate of the West Potrillo Basalt as observed
under crossed nicols. Mineralogy includes augite,
kaersutite, olivine and spinel. Magnification: 20X.

varies.   In   general, olivine when in contact with basalt
shows a sharp boundary.   On the other hand, clinopyroxene,
feldspar and spinel react with the basalt, often producing
corroded boundaries or glass.

Mineralogy

Pyroxene and Amphibole

The   pyroxene   in   the   inclusions   varies   from
greenish-grey augite to purplish titanaugite which shows a
40-45 degree extinction angle. In crystal aggregate xe-
noliths, the crystals are usually subhedral to anhedral
and vary in size from one to six millimeters. The clino-
pyroxene shows varying degrees of uralitization to kaersu-
tite, a titanium amphibole which is strongly pleochroic
from golden- to red-brown.   In crystal aggregates the
kaersutite ranges from one to seven millimeters and is
euhedral to anhedral. In some xenoliths a second pyroxene
(orthopyroxene) was noted exsolving from the augite.

The augite occurs both as megacrysts and in cry-
stal aggregates sometimes associated with olivine and/or
feldspar. The kaersutite occurs as megacrysts, as a re-
placement product of pyroxene and as in intercumulus phase
which is usually poikilitic.   Similar occurrences   are
noted by Best (1970) in Arizona.

Olivine

The olivine was determined to be ferroan forster-
ite by X-ray diffraction and scanning electron microscope
analysis. The crystals vary from anhedral to euhedral and
from less than one millimeter to three millimeters. The
olivine shows varying degrees of alteration to iddingsite.

Feldspar

Feldspar is found in less than 20 percent of the
crystal aggregate xenoliths in contrast to its relative
abundance as megacrysts. The feldspar in the xenoliths is
Na-laboradorite, which contrasts markedly with the compo-
sition of the megacrysts. In most cases the feldspar
makes up less than 10 percent of the rock (see Appendix
C), although two anorthosite inclusions were noted. These
anorthosite inclusions contain approximately 7-10 percent
K-feldspar.

It is interesting to note that a veinlet of
feldspar occurs in a kaersutite-rich inclusion (Plate 14).
Again, the feldspar in the veinlet is a calcic plagioclase
with minor K-Feldspar. One sample (64A) is also noteably
high (60 percent) in feldspar.

Oxides

Green spinel occurs as hercynite or pleonaste. The
spinel occurs as anhedral crystals commonly interstitial
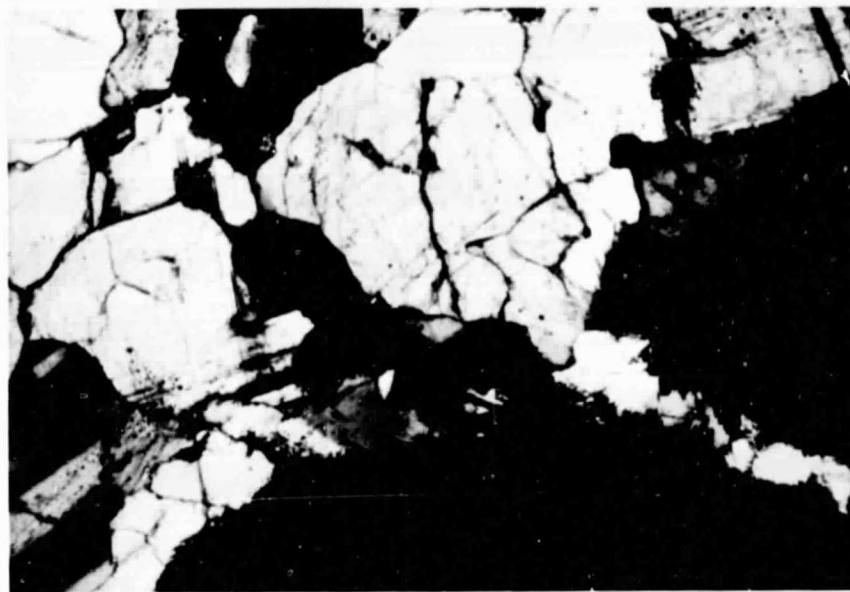
Plate 14. Veinlet of feldspar in kaersutite-
rich inclusion. Note slight reaction of the
feldspar with the kaersutite. The feldspar
could have been injected into the xenolith
after formation, or have been trapped fluid.
Observation under crossed nicols. Magnifica-
tion: 20X.

to the silicates but also as subhedral inclusions in pyroxene and amphibole (Plate 15).

Anhedral to euhedral black spinel is common. Much of the black mineral is ferrian spinel as determined by X-ray diffraction and semi-quanlitative X-ray flourescence analysis. Ferrian spinel is present in the crystal aggregate xenoliths and is also rarely found as megacrysts.. Titaniuim magnetite is also present and in some cases contains exsolved ilmenite. Large skeletal ilimenite crystals are common in come crystal aggregate samples (Plate 16).

A bright yellow isotropic mineral, perovskite(?) is abundant in a small percentage (5 percent) of the crystal aggregates. Black needle-like crystals (probably ilmenite) seem to have exsolved from the perovskite forming a trellis type intergrowth as described by Gorese/ (1976). The ilmenite was later partially oxidized to a red spinel (Plate 16 and Plate 17).

Glass

The inclusions have reacted with magma or partially melted to form yellow to orangish-brown intergranular glass (Plate 18) possibly as the magma came into contact with the inclusions located at lesser depth and thus cooler, or due to partial melting due to change in temperature and/or pressure. Microlites or quenched crystals
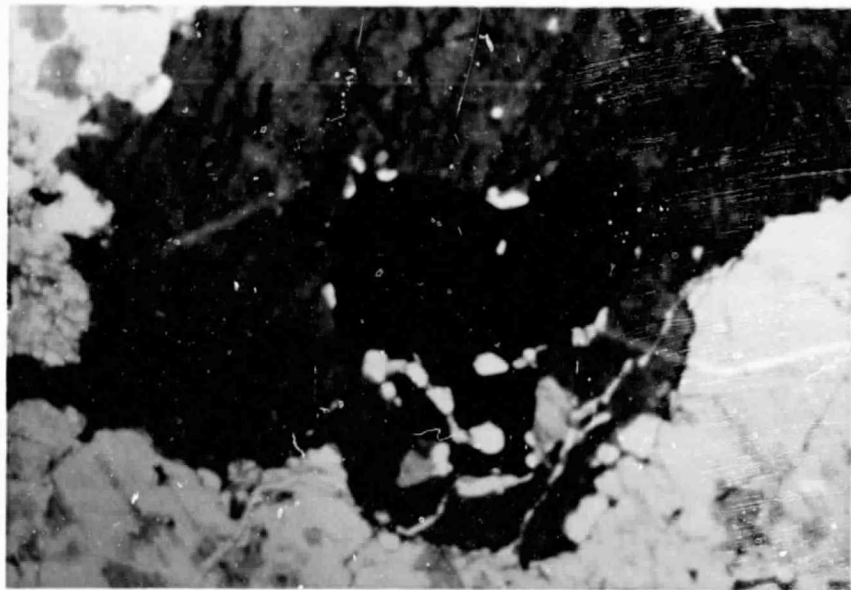
Plate 15. Anhedral hercynite in contact with
kaersutite in ultramafic inclusion of the West
Potrillo Basalt observed under uncrossed nicols.
Magnification 20X.
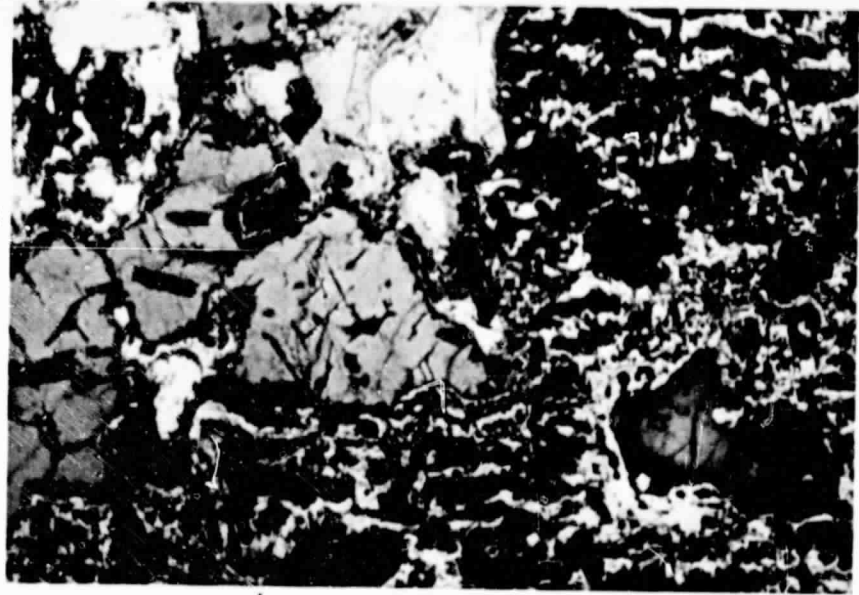
Plate 16. Skeletal ilmenite and yellow perov-
skite in ultramafic inclusion of the West Potrillo
Basalt as observed under uncrossed nicols.
Magnification 20X.

Plate 17. Perovskite (yellow) with exsolved
ilmenite forming trellis structure in ultramafic
xenolith of the West Potrillo Basalt as observed
under uncrossed nicols. Magnification: 80X.
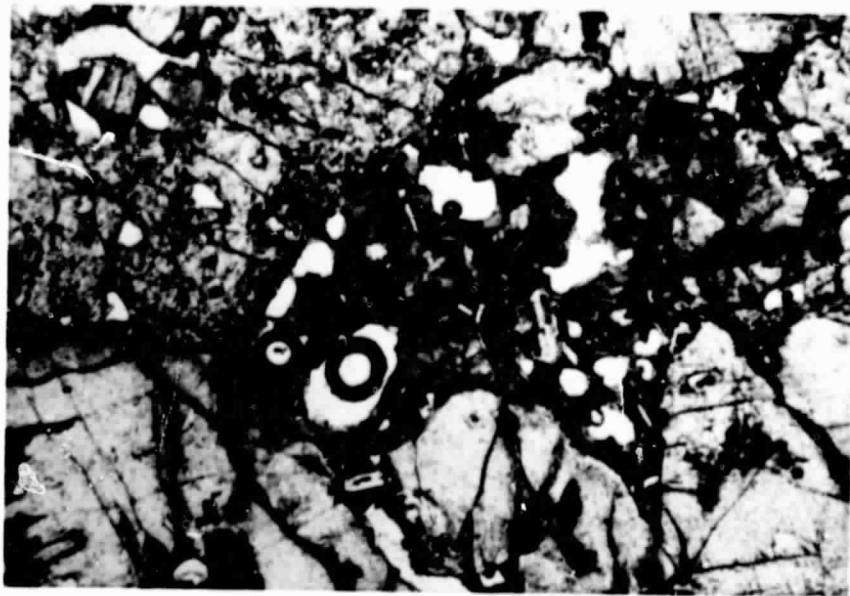
Plate 18. Glass (orangish-yellow) formed in
ultramafic xenolith of the West Potrillo Basalt.
Small microlites of olivine, pyroxene and felds-
par are observed in the glass. Observation with
uncrossed nicols. Magnification 20X.

of olivine, pyroxene and feldspar are sometimes present in
the glass.

Alteration

Various stages of alteration are observed in the
crystal aggregate xenoliths. These include: 1) recry-
stallization and exsolution, 2) strain and cataclasis and
3) replacement of pyroxene by amphibole, of olivine by
iddingsite and the alteration and oxidation of spinels.

Recrystallization has obscured the cumulate tex-
ture of some rocks even further. Minor orthopyroxene
exsolution lamallae in augite was noted in approximately
five percent of the ultramafic nodules (Plate 19). Exso-
lultion lamellae of ilmenite are present in both
perovskite and magnetite. Inhomogeneous extinction and
strain shadows are observed in the feldspar megacrysts
(Plate 4).

The replacement of pyroxene by amphibole seems to
have taken place at depth, although not necessarily as a
result of reaction with a fluid. A complete transforma-
tion of the pyroxene to amphibole appears first along
cleavage traces followed by development of amphibole
cleavage and gradual uralitization of the entire crystal
(Plate 20). This sequence indicates an addition of water
to the environment of formation or a change in environment
after or during formation. The kaersutite has short,

Plate 19. Exsolution of orthopyroxene in some
augite grains in ultramafic inclusion of the West
Potrillo Basalt as observed under crossed nicols.
Magnification 20X.

Plate 20. Augite altering to brown kaersutite in
ultramafic xenolith of the West Potrillo Basalt,
observed under uncrossed nicols. Magnifica-
tion: 20X.

stubby crystals which form pseudomorphs after the original pyroxenes.

Olivine is commonly replaced by iddingsite as a result of exposure to volcanic gases during eruption. The alteration and oxidation of oxides to hematite or maghemite seems also to have taken place during eruption or shortly thereafter.

Classification

General

An ultramafic rock classification is given in Figure 5. The crystal aggregates of the West Potrillo Mountains listed in decreasing abundance include clinopyroxenites (35 percent), kaersutite-rich inclusions (24 percent), kaersutite-clinopyroxenites (13 percent), olivine clinopyroxenites (10 percent) and wehrlites (peridotites with a ratio of olivine to clinopyroxene of 3:1) (8 percent). Since the main constituents of the crystal aggregate xenoliths of the West Potrillo Mountains include pyroxene, kaersutite, olivine and spinel, a new classification scheme was devised (Fig. 6).

The inclusions of the West Potrillo Basalt fall into the Al-augite group of Wilshire and Shervais (1973) characterized by Al, Ti-rich augites, comparatively Fe-rich olivine and Al-rich spinel with notable kaersutite.
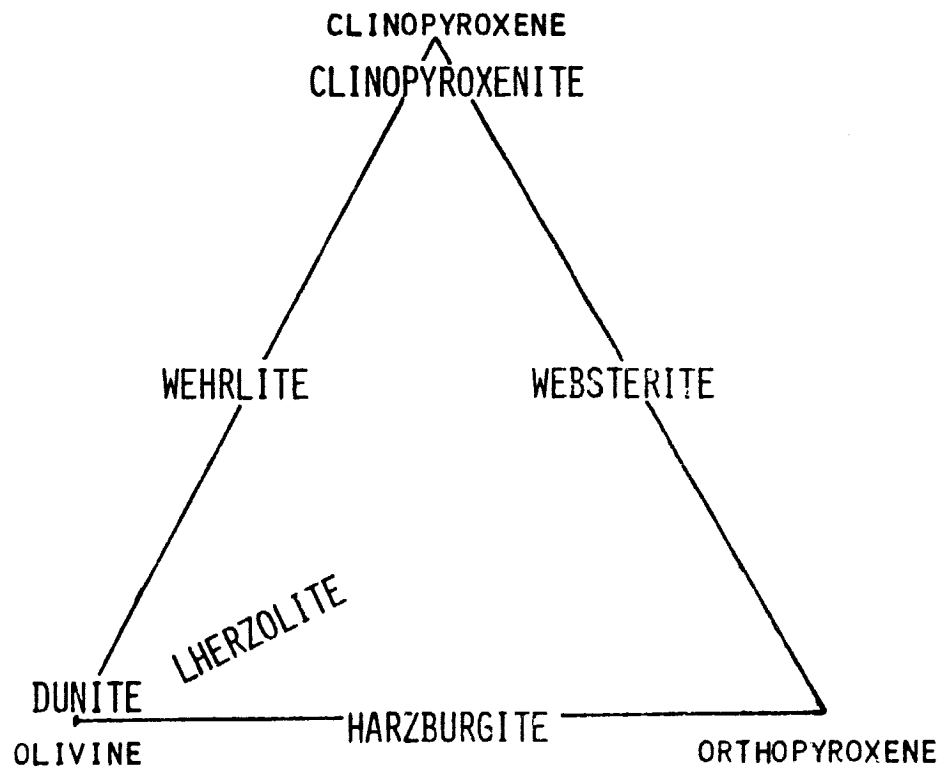
Fig. 5. Classification of ultramafic rocks (after Carter, 1970).
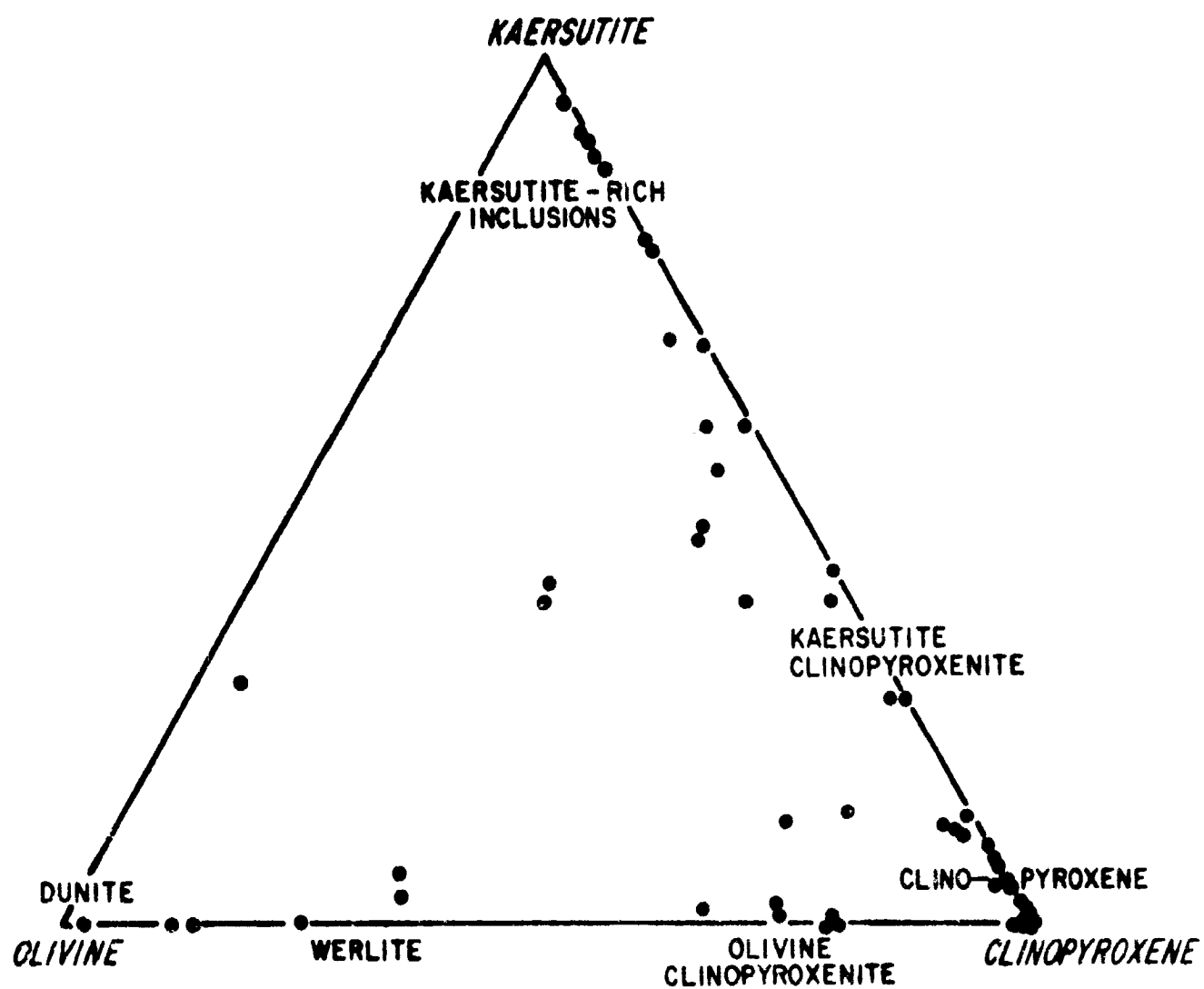
Fig. 6. Plot of representative crystal aggregate xenoliths of the West Potrillo Basalt, New Mexico.

Clinopyroxenite

Clinopyroxenites are the most abundant nodules occurring in the West Potrillo Mountains. They comprise approximately 35 percent of the crystal aggregates. Characteristic features of these inclusions include recrystallization features and the occurrence of perovskite. These inclusions contain abundant augite with lesser amounts of olivine, spinel, kaersutite and occasional plagioclase.

The clinopyroxene is greenish grey augite to purplish titanaugite and averages one millimeter to seven millimeters in diameter. Exsolution occurs in a small percentage of the augite grains. Olivine occurs as one to two millimeter anhedral crystals in about one third of the clinopyroxenites. Plagioclase is uncommon but when present is less than five percent. Kaersutite may make up 10 percent of the rock occurring both as an alteration product of augite and as an intercumulus phase. Black spinel commonly forms schiller structure in the larger augite grains. Green spinel occasionally occurs in very small anhedral grains.

Kaersutite-rich Inclusions

Kaersutite-rich inclusions (kaersutitites) make up 24 percent of the nodules and are characterized by having kaersutite in greater percentage than olivine or pyroxene.

Commonly one to two millimeter kaersutite grains are associated with minor olivine or pyroxene. Plagioclase is often an intercumulus phase in this type inclusion. Large grains often enclose minor olivine or smaller kaersutite grains. Minor reddish-brown mica is common. Black spinel is common, making up as much as 20 percent of the rock.

Kaersutite-clinopyroxenite

Kaersutite-clinopyroxenite crystal aggregates are very similiar to the clinopyroxenites, except kaersutite is much more abundant comprising as much as 40 percent of the inclusion. The kaersutite occurs both as anhedral interlocking grains associated with pyroxene, as an intercumulus phase (Plate 10) and as an alteration product of augite. Black spinel is slightly more common in these inclusions than in the clinopyroxenites. Kaersutite-clinopyroxenites comprise approximately 13 percent of the crystal aggregates.

Olivine-clinopyroxenite

Olivine-clinopyroxenites comprise 10 percent of the crystal aggregate xenoliths. Clinopyroxene crystals range in size from less than one millimeter to six millimeters with orthopyroxene exsolution noted. Olivine makes up as much as 30 percent of the inclusions. It occurs as anhedral crystals approximately one millimeter

in diameter. Kaersutite is present as an alteration product of augite. Plagioclase is uncommon and where present makes up less than five percent of the inclusion; it typically occurs as one to two millimeter anhedral crystals. Black spinel makes up approximately 20 percent of some inclusions and anhedral green spinel was noted in one inclusion.

Wehrlite

The least abundant inclusion type (except dunites and anorthosites) are the wehrlites; they comprise only 8 percent of the crystal aggregate xenoliths. Intercumulus plagioclase is present in small amounts (less than five percent). Kaersutite is present in small amounts as an alteration product of augite. Black spinel makes up 15 percent of some inclusions and green spinel is very minor. The two spinels are not found together in the same inclusion.

Other Crystal Aggregate Xenoliths

Three dunite inclusions were collected and described. These nodules contain an average of 90 percent olivine with minor black spinel, clinopyroxene and kaersutite and are polygonal in texture. Grains range from less than one millimeter to two millimeters averaging one millimeter. Alteration of olivine to iddingsite is common.

Two anorthosite crystal aggregate xenoliths were collected. The feldspar is Na-labordorite with approximately 10 percent K-feldspar. Cumulus texture is almost totally obscured and crystals are cracked and strained.

Chemistry of Crystal Aggregate Xenoliths

Eight samples were analysed by NASA using X-ray fluorescence including four kaersutite-clinopyroxenites, one kaersutite-rich inclusion, three clinopyroxenites and one clinopyroxenite with approximately 40 percent spinel. Analyses are presented in Table 4.

Compositions of the amphibole and the pyroxene in both crystal aggregate form and megacryst form were compared by X-ray fluorescence at the University of Texas at El Paso. Two kaersutite megacrysts, one kaersutite crystal aggregate, one megacryst of augite and one crystal aggregate of augite were analysed. Results are presented in Table 5. Both kaersutite and augite are of essentially the same composition whether found in aggregate or megacryst form. The kaersutite is noteably high in K_2O (1.17 to 1.43 percent) compared to other reported kaersutites as well as being high in titanium. The pyroxene was confirmed as consisting of augite. Na_2O is noticibly higher in the augite than in other reported augites. The augite is also slightly higher (one to two percentage points) in Al_2O_3 and CaO and slightly lower in MgO and SiO_2. The

TABLE 4

CHEMICAL ANALYSES OF MAFIC AND ULTRAMAFIC INCLUSIONS,
WEST POTRILLO BASALT

Analyzed at the National Aeronautics and Space Administration
Laboratory, Houston, Texas, using X-ray fluorescence.

Sample	59	60	61	492	13A
SiO_2	40.72	39.57	41.02	36.33	45.54
TiO_2	2.29	4.49	3.47	1.73	1.47
Al_2O_3	13.03	13.59	14.60	9.06	8.88
Fe_2O_3	8.42	10.19	7.90	17.01	3.50
FeO	3.64	1.61	3.78	1.73	4.99
MnO	0.20	0.17	0.17	0.35	0.16
MgO	11.57	12.47	10.98	14.30	16.02
CaO	16.75	12.93	14.89	13.75	17.26
Na_2O	1.49	2.15	1.72	0.92	0.88
K_2O	0.26	1.10	0.83	0.22	0.19
P_2O_5	0.20	0.16	0.29	1.15	0.08
S	0.00	0.04	0.04	0.00	0.01
Total H_2O	0.61	0.79	1.12	1.87	0.79
TOTAL	99.18	99.25	100.83	98.43	99.76

Sample

59 Kaersutite-clinopyroxenite

60 Kaersutite-rich inclusion

61 Kaersutite-clinopyroxenite

492 Kaersutite clinopyroxenite

13A Clinopyroxenite

TABLE 4

			Continued		
Sample	15	27	29	53	20A-2*
SiO_2	14.39	44.88	44.07	42.57	38.96
TiO_2	1.23	1.36	1.43	1.76	2.89
Al_2O_3	42.07	8.52	7.74	11.96	18.01
Fe_2O	14.45	3.52	6.14	6.85	11.82
FeO	7.05	5.14	4.82	3.81	1.17
MnO	0.17	0.17	0.19	0.21	0.10
MgO	15.82	15.92	16.04	11.66	11.23
CaO	4.07	17.14	15.74	17.48	11.02
Na_2O	0.30	0.74	0.80	0.90	2.73
K_2O	0.12	0.15	0.32	0.32	1.56
P_2O_5	0.04	0.04	0.25	0.21	0.14
S	0.01	0.00	0.01	0.01	----
Total H_2O	0.61	1.70	1.36	1.31	0.95
TOTAL	100.33	99.27	98.90	99.06	100.58

Sample

15   Ferrian spinel clinopyroxenite

27   Clinopyroxenite

29   Clinopyroxenite

53   Kaersutite clinopyroxenite

20A-2 Kaersutite megacryst

* analyzed by Japan Analytical Chemistry Research Institute

TABLE 5

ANALYSES OF AMPHIBOLE AND PYROXENE INCLUSIONS, WEST POTRILLO BASALT

Analyzed at the University of Texas at El Paso using Ortec TEFA model 6110 X-ray energy dispersive fluorescence analyzer.

Sample	13B-4	56G	54A	222A	27A
SiO_2	36.43	36.98	34.86	46.13	47.13
TiO_2	6.09	5.79	6.78	1.82	1.38
Al_2O_3	12.72	10.55	11.46	6.94	6.85
$FeO*$	14.14	16.22	16.21	9.85	7.59
MnO	0.14	0.16	0.16	0.12	0.10
MgO	12.62	10.55	10.60	12.34	12.40
CaO	11.40	11.81	11.98	21.95	22.08
Na_2O	2.36	1.83	1.74	1.29	1.40
K_2O	1.43	1.35	1.16	0.14	0.33
P_2O_5	0.25	0.26	0.26	0.26	0.29
Total	97.50	96.47	95.21	100.84	99.55
	Kaer-sutite Mega-cryst	Kaer-sutite Mega-cryst	Kaer-sutite Crystal Aggregate	Augite Mega-cryst	Augite Crystal Aggregate

*Total Fe reported as FeO

relatively high alkali percent of the amphibole and augite and the high TiO_2 of the amphibole could reflect the nature of the host basalt which is also high in those constituents.

The mafic nodules and host basalt were analyzed for uranium, thorium and potassium utilizing gamma spectrometry. Uranium and thorium values from typical igneous rocks are (from Levinson, 1974):

Ultramafic	U-0.0001	Th-0.0003
Basalt	U-0.06	Th-2.2
Granodiorite	U-3.0	Th-10.0
Granite	U-4.8	Th-17.0

Table 6 includes a summary of results from the analyses of nine crystal aggregate xenoliths and two basalt samples. The uranium and thorium values from the basalts are approximately double the average contained in a typical basalt. Zartmen and Tera (1973) discuss the uranium, thorium and lead compositions of five peridotite inclusions of probable mantle origin. They note that a sample of basalt from the West Potrillo Basalt contains 1.11 parts per million uranium and 3.83 parts per million thorium. The ultramafic crystal aggregate xenoliths of the West Potrillo Mountains contain abnormally high U and Th averaging 5000+ times the amount normally expected from

TABLE 6

Gamma Spectrometry Results			
<u>Sample</u>	<u>Th (ppm)</u>	<u>U (ppm)</u>	<u>K (percent)</u>
42-EX Wehrlite	4.58	7.33	0.13
492 Spinel clinopyroxenite	2.22	1.52	0.17
68C Kaersutite clinopyroxenite	0.49	1.06	0.38
421P Kaersutite-rich inclusion	4.38	1.00	0.97
13G Clinopyroxenite	1.31	0.88	0.81
621F Kaersutite-rich inclusion	3.38	0.68	0.61
59C Clinopyroxenite	3.43	0.60	0.12
492D Spinel clinopyroxenite	2.69	0.59	0.10
65B Amphibole megacryst	1.04	0.46	1.04
382D Basalt	4.46	2.45	0.76
14D Basalt	3.47	1.74	1.31

Analysis carried out at the University of Texas at
El Paso.

ultramafic rocks. Roy (personal communication, 1979) sug-
gests some sort of relationship to kimerlite since kimber-
lite contains abnormally high uranium and thorium values.
Kimberlite also has high potassium, aluminum, titanium and
calcium as do the inclusions of the West Potrillo Basalt
and is formed at very great pressure.

DISSCUSSION

General

The long term time spans over which alkaline mag-
mas are emplaced within small areas, the deposition of
alkaline rocks in linear belts, and the presence of essen-
tially identical basalt in both ocean basins and con-
tinents, the common low initial Sr87/Sr86 ratios and the
low melting compositons all suggest that alkaline magma is
generated within the mantle and moves up into the crust
along recurrently opened fractures (Barker, 1974).

In basaltic rocks, mafic and ultramafic inclusions
are almost exclusively confined to the alkali basaltic
types. Therefore, it is assummed in this study that the
West Potrillo Basalt and associated inclusions are of man-
tle origin. The ultramafic inclusions of alkali basalt
have been studied intensely, for example, Lausen and Mura-
ta (1927), Richter (1961), Wilshire and Binns (1961), Kuno
(1963), Aoki (1968), Wilshire and Shervais (1973), Best
(1974, 1975), and Baldridge (1978). The most ubiquitous
inclusion type is gabbroic (mafic) in composition. The
most common ultramafic type in lherzolite (see Fig. 5).
However, in the West Potrillo Mountains the ultramafic
inclusions are generally rich in clinopyroxene and contain
abundant kaersutite with olivine, spinel and feldspar of

64

varying porportions and contain virtually no orthopyroxene (see Fig. 5 and Fig. 6).

Megacrysts

Feldspar Megacrysts

The occurrences of feldspar megacrysts in conjunction with eruptions of alkali basalts reported in the literature seem to have several things in common. The alkali basalt is relatively recent (Pliocene to recent) and the inclusions are associated with a pyroclastic event. The feldspar megacrysts are also associated with mafic and ultramafic inclusions (Laughlin and others, 1974).

Feldspar megacrysts have been noted in the Rio Grande rift near Truth or Consequences, New Mexico (Warren and others, 1979) and in the Black Range, a rift associated graben in southwestern New Mexico (Foder, 1978). Feldspar megacrysts are also noted in the San Bernadino volcanic field in southeastern Arizona (Lynch, 1978), at Bandera Crater near Grants, New Mexico (Laughlin and others, 1974), in the Old Dad Mountains in California (Wilshire and others, 1971), in northeastern New South Wales (Binns and others, 1970) and in Nigeria (Wright, 1968).

The megacrysts are larger in crystal size than the associated crystal aggregate rocks and apparently are not

broken relicts from polymineralic bodies. In fact, they seem to be phenocrysts. The presence of anorthoclase and K-oligoclase as phenocrysts in alkali basalts is reasonable because of the relatively high alkalis percentage in the basalt. The trend from andesine to anorthoclase could indicate a source from a differentiated magma that became progressively enriched in alkali elements during crystallization or simultaneous formation of two felspar groups, one K-feldspar and the other plagioclase. The normative feldspar compositions of the host basalt plot within the excluded portion of the Or-Ab-An diagram indicating that two types of feldspar, one alkali-rich and the other more calcic would have crystallized from the melt and co-existed in equilibrium at high temperature and pressure (Laughlin and others, 1974).

The feldspar megacrysts are of different composition than the feldspar in the crystal aggregates. Vitreous appearance and tendancy toward conchoidal fracture as well as high structural state (Hoffer and Hoffer, 1973) and no apparent zoning of the megacrysts all suggest formation at great depth for these crystals.

Binns and others (1970) cite numerous experimental studies which indicate the tendancy of plagioclase near the liquidous composition to become more sodic at high pressure (equivalent to 40 to 60 kilometers of depth). Nash (1973) used experimental data from the literature to

determine a relation between An content of plagioclase and the pressure under which it crystallized. He proposed:

$$P(kilobars)=-0.38(percent\ An)+34.7$$

where P is pressure and An percent is the percentage of anorthite in the plagioclase. According to the equation, the plagioclase megacrysts of the West Potrillo basalt formed at pressures ranging from 18.36 kilobars to 28.01 kilobars averaging 23.30 kilobars or approximately 75 kilometers of depth. That value seems extreme, yet consistant with tectonic rift association of the megacrysts.

Warren and others (1979) suggested that the formation of "anorthoclase" megacrysts in the Engle Basin was at less than 29 kilometers. The geologic occurrence of such crystals is similiar to that of the West Potrillo Basalt. When plotted on an Or-Ab-An diagram, the results and trends are strikingly similiar.

Kaersutite, Augite and Spinel Megacrysts

The compositions of kaersutite and augite grains is similiar in both crystal aggregates and megacrysts. These megacrysts, as with the feldspar megacrysts do not seem to have been separated from a polymineralic body. Their large size indicates formation at great depth or under reasonably high pressure-temperature conditions. Binns and others (1970) interpret megacrysts of pyroxene,

kaersutite and ferrian spinel as cognate precipitates formed at a pressure approximate to the crust-mantle boundary. It was noted that the host basalt is high in titanium oxide, aluminum oxide and high in total alkali. It is believed that those characteristics are reflected in the composition of the megacrysts which are also high in those constituents and which were most likely derived as phenocrysts within the host basalt.

Ultramafic Xenoliths

General

Wilshire and Shervais (1973) suggest two catagories for the classification of ultramafic xenoliths in basaltic rocks from the western United States. First is the Al-augite type composed of Al-, Ti-augite, comparatively Fe-rich olivine, orthopyroxene and Al-spinel. The second is the Cr-diopside type and is composed of Cr-diopside, Cr-spinel, and Mg-olivine and Mg-pyroxene. Virtually no chromium is detected in the inclusions of the West Potrillo Basalt.

Lherzolite (see Fig. 4) is the most common rock type of the Cr-diopside group. That group is generally considered to represent mantle material from which variable amounts of basaltic liquid has been removed (Wilshire and Shervais, 1973). The most common rock types of the Al-augite group include olivine-clinopyroxenite, wehrlite

and clinopyroxenite. Xenoliths of the Al-augite group are isotopically similiar to the host basalt unlike the Cr-diopside group (Steuber and Murthy, 1966). It is generally believed that the Al-augite group represents cognate cumulates and that the Cr-diopsidde group represents country rock in the mantle (Wilshire and Shervais, 1973; see Fig. 7).

Geobarametry and Geothermometry

Bordley and others (1971) postulate that if kaersutite is considered to be a Ti-K rich member of the pargasite-ferropargasite series then kaersutite plus Al-clinopyroxene can exist under conditions at 960-1015°C. If conditions are dry, titanium exsolves from kaersutite at about 10 kilobars. At 9-10 kilobars (25-35 kilometers of depth) and wet conditions at 900°C, a few plagioclase-bearing ultramafics are stable while at 960-1015°C ultramafics with kaersutite and clinopyroxene occur. At 1015°C, kaersutite stops forming and clinopyroxene forms. Therefore, the crystal aggregates of the West Potrillo Basalt probably formed at a depth approximating 25-35 kilometers under wet conditions. The plagioclase-bearing xenoliths forming at slightly lesser depths than the non-plagioclase-bearing xenoliths.

These estimates of pressure and temperature of formation fit well with the similiar occurrence of
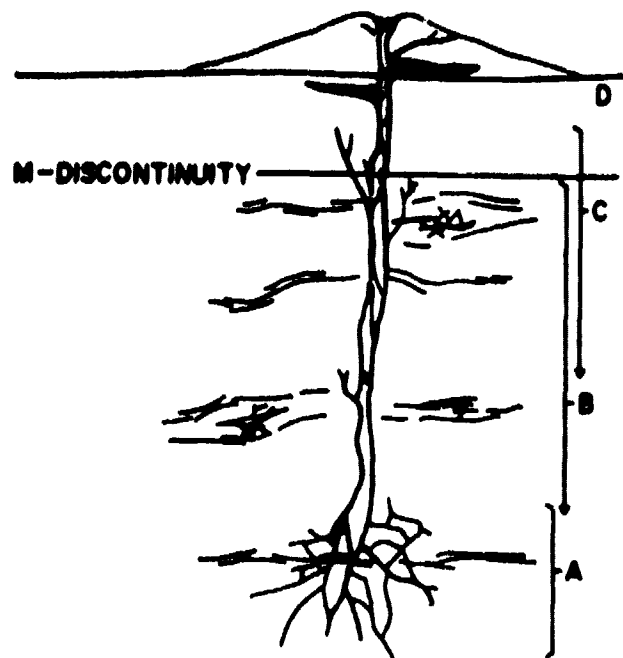
Fig. 7. Schematic diagram illustrating possible relationships of cognate Al-augite pyroxenite and Cr-diopside ultramafic groups. (A) Mantle source zone; anatomosing feeders to main conduits. Al-augite ultramafic xenoliths with complex vein networks represent earlier melts and wall rock from this and higher zones. (B) Gneissic mantle material composed of penetratively deformed Cr-diopside peridotites. Augen preserve parts of former complex vein networks, or, complex vein systems occur locally in rock bodies dominated by plane parallel lithologic layering. Depending on depth in mantle, these may belong to the Cr-diopside, garnetiferous, or feldspathic ultramafic groups. (C) Offshoot veins from the main conduits penetrate crystal and mantle rock that was not involved in the youngest melting episode. Xenoliths from this horizon include veins in peridotite of the Cr-diopside and feldspathic ultramafic groups. (D) Sill injections in upper curst and within contemporaneous volcanic pile yield cumulate differentiates that form locally important members of xenolith suites (Wilshire and Shervais, 1973).

inclusions in the Engle Basin. Warren and others (1979) suggest the following depths of formation of inclusions in the Engle Basin located within the Rio Grande rift:

Lherzolite	36-42 kilometers
Pyroxenite	32-36 kilometers
Granulite	29-32 kilometers
Feldspar megacrysts	less than 29 kilometers

They suggest that a similar petrologic sequence of pyroxenite, megacrysts and granulite may be a characteristic subcrustal feature of the Rio Grande rift. An increase in the Fe/Mg and Na/Ca ratios upward is noted in the sequence.

Tectonic Implications

A regional gravity high of +25 milligals which is typical of rift valleys and an unreversed refraction profile confirms the presence of anamolous mass excess between 27 and 35 kilometers depth, near the base of the crust along the Rio Grande rift in southern New Mexico (Cook and others, 1979). The mass excess could be abnormally dense lower crust or abnormally hot, low density intruded mantle or a mantle diapir.

Everson and Silver (1978) report highly radiogenic lead in volcanic rocks of Pliocene and Pleistocene age

such as the West Potrillo Basalt, which is similiar to the radiogenic lead reported on oceanic islands. They have also suggested a deep mantle upwelling in the southern portion of the Rio Grande rift as a source of the the basalt.

Wilshire and Pike (1975) note that ultramafic xenoliths in basalt of the western United States are dominantly spinel-lherzolite which is an uncommon rock type in the West Potrillo Mountains. However, they note a similarity of such xenoliths and those related to them to alpine peridotite and suggest derivation of such crystals by partial fusion over a range of temperature and pressure conditions during diapiric rise of a portion of the upper mantle. Based on cross-cutting evidence, the following crystallization sequence of xenoliths is proposed by Wilshire and Pike. A chromium-diopside spinel pyroxenite (websterite) similiar in composition to the host lherzolite is the oldest rock type. Al-Ti augite pyroxenite, olivine clinopyroxenites and wehrlites with Al-spinel follow. Next in the sequence is kaersutite pyroxenite and lherzite and finally the gabbroid xenoliths (see Fig. 8). The xenoliths of the West Potrillo Basalt would correlate with the middle two catagories.

Baldridge (1973), studied mafic and ultramafic crystal aggregate xenoliths and megacrysts from volcanics at Abiquiu, Cienequilla and Elephant Butte, New Mexico,

Fig. 8. Schematic diagrams illustrating mantle diapirism with diapirism terminated at different levels in the lithosphere by volcanic eruptions (1 to 3) or by alpine mode of emplacement not necessarily associated with vol- canism (4). Volcanic and xenolithic products may vary with level of termination as noted. This figure does not represent a sequence of events in a single diapir. (After Wilshire and Pike, 1975).

1. Diapirism terminated by kimberlitic erup- tion. Beginning of melting, perhaps in a heterogeneous starting material. Separation of liquids from which kimberlite-suite and pyroxenite crystallizes (pryoxenite+garnet+ phlogopite). Liquids melilitite?

2. Diapirism terminated by nepheline basanite- basanite eruptions. More extensive melting than in kimberlite, including remelting of older dikes. Crystallization of Cr-diopside spinel pyroxenite (+phlogopite) and garnet pyroxenite in higher T-P region; crystalliza- tion of Al-Ti augite pyroxenite, wehrlite, kaersutite pyroxenite, and lherzite in lower T-P regions. Local pockets of liquid give rise to cumulate units, but liquids range to ultramafic. Possible transformation of garnet lherzolite to spinel lherzolite in higher T-P region. Sequential modification of early- crystallized partial melts by deformation, re- crystallization, and partial remelting.

3. Diapirism terminated by alkalic basalt eruption after diapir penetrates lower crust. Separation of liquids (from all pre-existing rocks) from which pryoxenite and gabbroid of the alkalic-subalkalic basalt suite crystallize as dikes. Local pockets of liquid give rise to cumulate units. Unmixing, deformation, re- crystallization, remelting with last melts quenched by eruption.

4. Alpine peridotite. Variety of dikes formed sequentially in spinel and garnet pyroxenite to gabbroid. All deformed and at least partly recrystallized.
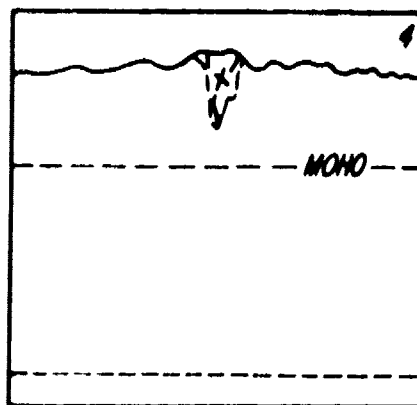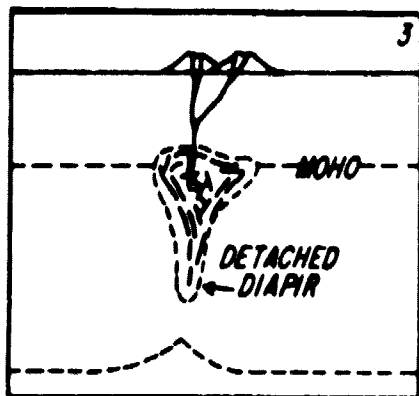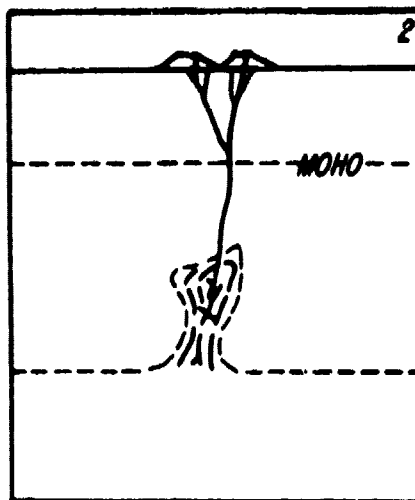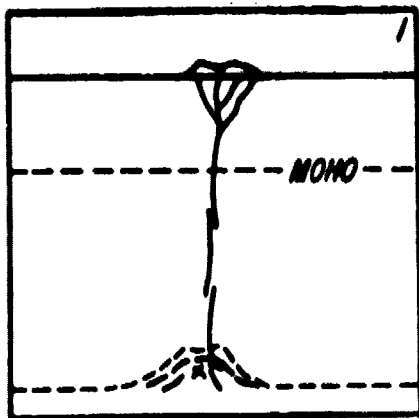
also located within the Rio Grande rift and has concluded that these lithic inclusions represent fragments of several separate intrusive bodies of different bulk composition which were originally located at different depth within the lithosphere. He suggests that such inclusions may be part of a wedge of mafic rocks emplaced into the lithosphere above a mantle diapir associated with rifting, whereas megacrysts could be phenocrysts or dissaggreated pegmatite.

Geophysical and geological evidence supports a model of mantle upwelling beneath the southern Rio Grande rift.

CONCLUSIONS

Megacrysts of the West Potrillo Basalt are inter-
preted as being phenocrysts of the host basalt which
formed at great depth. The phenocrysts formed as stable
phases at great temperature and pressure. The host basal-
tic liquid changed composition as it rose toward the sur-
face as evidenced by the partial reaction of inclusions
with the basalt to produce rounded, embayed and corroded
crystal boundaries.

The mafic and ultramafic crystal aggregates appear
to be chemically related to an alkalic basalt generated in
the mantle though not necessarily representing the host.
The crystal aggregates of the West Potrillo Basalt are of
cumulate origin and could represent more than one cumulus
body located at different levels in the upper mantle or
lower crust at approximately 25-35 kilometers of depth,
very near the crust-mantle boundary. The varying mineral
assemblages represent slightly different temperature and
pressure conditions. Individual cumulate bodies have
undergone some degree of metamorphism at depth.

REFERENCES

Aoki, K., 1963, The kaersutites and oxykaersutites from
        alkalic rocks of Japan and surrounding areas:
        Jour. Pet., v. 4, part 2, p. 198-210.

Aoki, K., 1968, Petrogenesis of ultrabasic and basic in-
        clusions in alkali basalts, Iki Island, Japan:
        Am. Min., v. 53, p. 241-256.

Baldridge, W.D., 1978, Mafic and ultramafic inclusions
        from the Rio Grande Rift and their bearing on
        the composition and thermal state of the litho-
        sphere (abs.), in 1978 International Symposium
        on the Rio Grande Rift Program and Abstracts,
        Los Alamos Scientific Laboratory, p. 15-16.

Barker, D.S., 1974, Alkaline rocks of North America in
        The Alkaline Rocks, H. Sorensen, Ed., John Wiley
        and Sons, p. 160-171.

Bersch, M.G., 1977, Petrography and Geology of the
        Southern West Potrillo Basalt Field, Dona Ana
        County, New Mexico, unpub. Masters thesis, Univ.
        Texas at El Paso, 60p.

Best, M.G., 1970, Kaersutite-peridotite inclusions and
        kindred megacrysts in basanitic lavas, Grand Can-
        yon Arizona: Contr. Min. Pet., v. 27, p. 25-44.

Best, M.G., 1974, Mantle-derived amphibole within inclu-
        sions in alkalic-basaltic lavas: J. Geophys. Res.,
        v. 79., p. 2107-2113.

Best, M.G., 1975, Amphibole-bearing cumulate inclusions,
        Grande Canyon, Arizona and their bearing on silica-
        undersaturated hydrous magmas in the upper mantle:
        J. Pet., v. 16, p. 212-230.

Binns, R.A., Ouggan, M.B., and Wilkinson, J.F.G., 1970,
        High Pressure Megacrysts in alkaline lavas from
        northeastern New South Wales: Am. J. Sci., v. 269,
        p. 132-168.

Bowers W.E., 1960, Geology of the East Potrillo Moun-
        tains, M.S. thesis, Univ. of New Mexico, 67p.

Carmichael, J.S.E., Turner, F.J., and Verhoogen, J., 1974,
        Igneous Petrology, McGraw-Hill Book Company.

Carter, J.L., 1970, Mineralogy and chemistry of the earth's upper mantle based on partial fusion-partial crystallization model: G.S.A. Bull., v. 81, p. 2021-2034.

Chapin, C.E., 1971, The Rio Grande rift, part 1: Modification and additions, in Guidebook to San Luis Basin, New Mexico, Geol. Soc. Field Conf. Guidebook 22, p. 191-201.

Chapin, C.E., 1979, Evolution of the Rio Grande rift-a summary in Rio Grande Rift: Tectonics and Magmatism, Robert E. Riecker, ed.: Am. Geophys. Union spec. pub., p. 195-208.

Dawson, J.B., 1967, Geochemistry and origin of kimberlite in Ultramafic and Related Rocks, Peter J. Wyllie, ed., John Wiley and Sons, Inc., p. 269-278.

Deer, W.A., Howie, R.A., and Zussman, J., 1963, Rock-Forming Minerals, vol. 2, Chain Silicates, Longman (pub.).

Deer, W.A., Howie, R.A., and Zussman, J., 1977, An Introduction to the Rock Forming Mineral, Longman (pub.).

Everson, J.E., and Silver, L.T., 1978, Lead systematics of late Cenozoic basalts from the Rio Grande rift, Los Alamos Sci. Lab. Conf. Proceedings, LA-7487-C, p. 36-37.

Fenneman, N.M., 1931, Physiography of the Western United States, McGraw-Hill, Inc., New York, 534p.

Foder, R.V., 1978, Ultramafic and mafic inclusions and megacrysts in Pliocene basalt, Black Range, New Mexico: G.S.A. Bull., v. 89, p. 451-459.

Goresey, A.E., Hagerty, S.E., Huebner, J.S., Lindsley, D.H., and Rumble, D., Oxide Minerals, D. Rumble, ed.: Min. Soc. Am. Short Course Notes, v. 3, Southern Printing Co.

Grew, E.S., 1979, Al-Si disorder of K-feldspar in crustal xenoliths at Kilbourne Hole, New Mexico, Am. Min., v. 64, p. 912-916.

Hawley, J., and Kottlowski, F.E., 1969, Quaternary
geology of the southcentral New Mexico border
region in Border stratigraphy Symposium, F.E.
Kottlowski and D.V. LeMone (eds.), New Mex. Bur.
Mines and Min. Res., Circ. 104, p. 89-104.

Heinrich, E.W., 1965, Microscopic Identification of
Minerals, McGraw-Hill Book Co.

Hoffer, J.M., 1973, Quaternary basalts of the West
Potrillo Mountains, south-central New Mexico.
El Paso Geol. Soc. Guidebook 7, p. 26-32.

Hoffer, J.M., 1976, Geology of Potrillo Basalt Field,
South-central New Mexico, New Mex. Bur. Mines
and Min. Res., Circ. 149, 30p.

Hoffer, J.M., and Hoffer, R.L., 1973, Composition and
structural state of feldspar inclusions from
alkali olivine basalt, Potrillo Basalt, southern
New Mexico, G.S.A. Bull., v. 84, p. 2139-2142.

Holloway, J.R., 1973, The system pargasite-H_2O-CO_2: a
model for melting of a hydrous mineral with a
mixed-volatile fluid-I. Experimental result to
8Kbar: Geochim. Cosmochim. Acta, v. 37, p 651-666.

Irvine, T.N., 1967, The Duke Island Ultramafic complex,
southeastern Alasks in Ultramafic and Related
Rocks, Peter J. Wyllie, ed., John Wiley and
Sons, Inc., p. 84-97.

King, W.E., Hawley, J.W., Taylor, A.M., and Wilson, R.P.,
1969, Hydrogeology of the Rio Grande valley and
adjacent intermontane areas of southern New
Mexico: Water Resources Inst., Rept. 6, New
Mexico State Univ., 141p.

Kuno, H., 1953, Mafic and ultramafic nodules in basaltic
rocks of Hawaii: G.S.A. memoir 115, p. 189-231.

Laughlin, A.W., Brookins, D.G., Kudo, A.M., and Causey,
J.D., 1971, Chemical and strontium isotopic inves-
tigations of ultramafic inclusions and basalt,
Bandera Crater: Geochim. Cosmochim. Acta, v. 35,
p. 107-113.

Laughlin, A.W., Manzer, G.K., Jr., and Carden, J.R., 1974,
Feldspar megacrysts in alkali basalts, G.S.A.
Bull., v. 85, p. 413-416.

Lausen, C., 1927, The occurrence of olivine bombs near
        Globe, Arizona, Am. J. Sci., v. 14, p. 293-306.

Levinson, A.A., 1974, Introduction to Exploration Geo-
        chemistry, Applied Pub. Ltd., Calgary, p. 43-47.

Lynch, D.J., 1978, The San Bernadino volcanic field of
        southeastern Arizona, New Mex. Geol. Soc.
        Field Conf. Guidebook 29, p. 261-268.

MacGregor, I.D., 1968, Mafic and ultramafic inclusions
        as indicators of the depth of origin of basaltic
        magmas: J. Geoph. Res., v. 73, p. 3737-3747.

MacGregor, I.D., 1974, The system $MgO-Al_2O_3-SiO_2$:Solu-
        bility of Al_2O in enstantite for spinel and
        garnet peridotite compositions: Am. Min.,
        v. 59, p. 110-119.

MacGregor, I.D., and Basu, A.R., 1976, Geological pro-
        blems in estimating mantle geothermal gradients:
        Am. Min., v. 61, p. 715-724.

Mason, B., 1968, Kaersutite from San Carlos, Arizona,
        with comments on the paragenesis of this mineral:
        Min. Mag., London, v. 36, p. 997-1002.

Mercier, J.C., and Carter, N.L., 1975, Pyroxene Geotherms:
        J. Geophys. Res., v. 80, p. 3349-3362.

Mercier, J.C., 1976, Single pyroxene geothermometry and
        geobarametry: Am. Min., v. 61, p. 603-615.

Millican, R.S., 1971, Geology and petrography of the Ter-
        tiary Mt. Riley-Cox pluton, Dona Ana County, New
        Mexico, M.S. thesis, Univ. of Texas at El Paso
        87p.

Mori, T., 1977, Geothermometry of spinel lherzolites:
        Cont. Min. Pet., v. 59, p. 261-279.

Muir, I.D., and Tilley, C.E., 1961, Mugearites and their
        place in alkaline igneous rocks series: J. Geol.,
        v. 69, p. 186-203.

O'Hara, M.J., 1967, Mineral paragenesis in ultrabasic
        rocks in Ultramafic and Related Rocks, Peter
        J. Wyllie, ed., John Wiley and Sons, Inc.,
        p. 393-403.

Padovani, E.R., and Carter, J.L., 1977, Aspects of the deep crustal evolution beneath south central New Mexico in The Earth's Crust, J.G. Heacodk, ed., Am. Geoph. Union Geoph. Monograph 20, p. 19-55.

Padovani, E.R., 1978, Deep crystal evolution beneath south central New Mexico: constraints on the geothermal gradient from xenolithic assem- blages (abs.), in International Symposium on the Rio Grande Rift Program and Abstracts, Los Alamos Sci. Lab., p. 66-67.

Page, R.O., 1973, Stratigraphy and Sructure of the Qua- ternary Malpais Maar Volcano, Dona Ana County, New Mexico, M.S. thesis, Univ. Texas at El Paso, 46p.

Pike, J.E.N., and Schwarzman, E.C., 1977, Classification of textures in ultramafic xenoliths: J. Geol., v. 59, p. 472-489.

Reid, J.B., Jr., 1978, The petrologic history of the upper mantle beneath the southern Rio Grande rift with speculation on limits to Cenozoic diapirism beneath the rift (abs.), in 1978 Inter- national Symposium on the Rio Grande Rift Program and Abstracts, Los Alamos Sci. Lab., p. 72.

Renault, J.R., 1970, Major element variations in the Potrillo, Carrizozo and McCartys basalt fields, New Mexico: New Mex. Bur. Mines and Min. Res. Circ. 113, 22p.

Richter, D.H., and Murata, K.J., 1961, Xenolithic nodules in the 1800-1801 Kaupulehu flow of Hualalai Vol- cano: U.S.G.S. Prof. Paper 424-B, p. 215-217.

Salvenson, J.O., 1978, Variations in the Geology of rift basins-a tectonic model in 1978 International Symposium on the Rio Grande Rift Program and Abstracts, Los Alamos Sci. Lab., p. 82-86.

Saxena, S.K., 1976, Two-pyroxene geothermometer, a model with an approximate solution: Am. Min., v. 61, p. 6433-652.

Seager, W.R., and Morgan, P., 1979, Rio Grande rift in
southern New Mexico, West Texas, and northern
Chihuahua in Rio Grande Rift: Tectonics and Mag-
matism, Robert E. Reicker, ed.: Am. Geoph.
Union Spec. Pub., p. 87-106.

Steuber, A.M., and Murthy, V.M., 1966, Strontium isotope
and element abundances in ultramafic rocks: Geo-
chim. Cosmochim. Acta, v. 30, p. 1243-1259.

Stoesser, D.B., 1973, Mafic and Ultramafic Xenoliths of
Cumulus Origin, San Francisco Volcanic Field,
Arizona, unpub. Ph.D. Disser., Univ. Oregon, 260p.

Stoesser, D.B., 1974, Xenoliths of the San Francisco vol-
canic field, northern Arizona, in Geology of
Northern Arizona, Pt. II, Area studies and field
guides: G.S.A., p. 530-545.

Upton, B.G.J., 1967, Alkaline Pyroxenites in Ultramafic
and Related Rocks, Peter J. Wyllie, ed., John
Wiley and Sons, Inc., p. 281-288.

Wager, L.R., Brown, G. M., and Wadsworth, W.J., 1960,
types of Igneous Cumulates, J. Pet. v. 1, p 73-85.

Warren, R.G., Kudo, A.M., and Keil, K., 1979, Geochemistry
of lithic and single crystal inclusions in basalt
and a characterization of the upper mantle-lower
crust in the Engle Basin, Rio Grande rift, New
Mexico in Rio Grande Rift: Tectonics and Magma-
ism, Robert E. Reicker, ed.: Am. Geoph. Union
spec. pub., p. 393-415.

Wilkinson, J.F.G., 1974, The mineralogy and petrography
of alkali basaltic rocks in The Alkaline Rocks,
H. Sorensen, ed., John Wiley and Sons, p. 67-95.

Wilshire, H.G., and Binns, R.A., 1961, Basic and ultra-
basic xen liths from volcanic rocks of New South
Wales, J. Pet., v. 2, p. 185-208.

Wilshire, H.G., Clark, L.C., and Schwarzman, E.C., 1971,
Kaersutite--a product of reactin between parga-
site and basanites at Dish Hill, California, Earth
Planet. Sci. Letters, v. 10, p. 281-284.

Wilshire, H.G., and Pike, J.E.N., 1975, Upper mantle diapirism: Evidence from analogous features in alpine peridotite and ultramafic inclusions in basalt, Geol., v. 3, p. 467-470.

Wilshire, H.G., and Shervais, J.W., 1973, Al-augite and Cr-diopside ultramafic xenoliths in basaltic rocks from Western United States, Phys. Chem. of the Earth, v. 9, p. 257-272.

Wright, J.B., 1968, Deep crustal origin for oligoclase and andesine phenocrysts in basalt from Gombe, Nigeria: Nature, v. 218, p. 262-263.

Zartman, R.E., and Terra, R., 1973, Lead conentration and isotope composition in peridotite inclusions of probable mantle origin: Earth and Planet. Sci. Letters, v. 20, p. 54-66.

Zimmerman, C., and Kudo, A.M., 1979, Geochemistry of andesites and related rocks, Rio Grande rift, New Mexico in Rio Grande Rift: Tectonics and Magmatism, Robert E.k Riecker, ed.: Am. Geoph. Union Spec. Pub., p. 87-106.

APPENDIX A

Summary of the Number and Type of Major Mineral
Constituents in Samples Collected. Map No. refers
to Sample Location map, Plate 1.

Sample No	Map No	Location	Feldspar	Pyroxene	Amphibole/ Pyroxene
11	84	SW¼, Sec 18 T28S, R2W	0	0	0
12	25	NE¼, Sec 24 T27S, R3W	6	2	0
121	25	NE¼, Sec 24 T27S, R3W	8	4	0
13	37	NE¼, SW¼, Sec20 T27S, R3W	26	2	6
131	37	NE¼, SW¼, Sec20 T27S, R3W	8	10	8
14	38	SW¼, SW¼, Sec19 T27S, R3W	6	2	0
141	38	SE¼, SE¼, Sec24 T27S, R3W	16	2	8
143	38	E½, Sec 27 T27S, R4W	2	0	4
144	38	E½, Sec 27 T27S, R4W	6	0	0
145	38	E½, Sec 27 T27S, R4W	12	0	2
15	38	SW¼, SE¼, Sec24 T27S, R4W	2	2	0
16	49	W½, Sec 31 T27S, R4W	0	0	0
173	50	SE¼, Sec 30 T27S, R4W	6	6	4
19	27	SW¼, Sec 23 T27S, R3W	4	0	10

Sample No	Map No	Location	Feldspar	Pyroxene	Amphibole/ Pyroxene
20	28	SW¼, Sec 22 T27S, R3W	6	8	10
201	28	NW¼, Sec 27 T27S, R3W	2	0	6
21	19	NW¼, Sec 4, T27S, R3W	2	0	6
221	21	NE¼, Sec 4 T27S, R3W	2	12	10
222	21	NE¼, Sec 4 T27S, R3W	8	0	4
23	20	SE¼, Sec 4 T27S, R3W	12	0	8
241	85	SE¼, Sec 34 T28S, R3W	0	0	4
242	85	SW¼, Sec 34 T28S, R3W	0	0	8
25	86	NW¼, Sec 2 T29S, R3W	0	0	0
26	87	SE¼, Sec 36 T28S, R3W	0	0	0
27	68	SW¼, Sec 35 T28S, R4W	0	0	14
28	72	SE¼, Sec 11 T29S, R4W	10	14	6
281	72	SE¼, Sec 11 T29S, R4W	6	2	2
282	72	SE¼, Sec 11 T29S, R4W	4	0	2
291	74	NW¼, Sec 7 T29S, R3W	0	0	6
292	74	SW¼, Sec 6 T29S, R4W	0	4	0

Sample No	Map No	Location	Feldspar	Pyroxene	Amphibole/ Pyroxene
292A	74	SW¼, Sec 6 T29S, R3W	8	0	2
301	71	SE¼,SW¼,Sec1 T29S, R4W	0	4	8
302	71	SW¼,SE¼,Sec1 T29S, R4W	0	0	8
31	69	NE¼, Sec 1 T29S, R4W	0	0	4
32	67	SW¼, Sec 36 T29S, R4W	10	0	0
33	81	SE¼, Sec 17 T28S, R3W	22	0	6
34	61	SE¼, Sec 18 T28S, R3W	4	0	6
35	60	SE¼, Sec 13 T28S, R4W	8	0	0
36	82	N½, Sec 15 T28S, R3W	4	0	8
37	83	SE¼, Sec 14 T28S, R3W	4	0	4
381	41	NW¼,NW¼,Sec25 T27S, R4W	8	0	8
382	41	SW¼,SW¼,Sec24 T27S, R4W	6	0	2
39	39	N½,SE¼,Sec 23 T27S, R4W	6	0	4
40	40	N¼, Sec 26 T27S, R4W	0	0	22
41	43	SE¼, Sec 27 T27S, R4W	0	0	0
42	44	SE¼,NW¼,Sec35 T27S, R4W	0	0	6

Sample No	Map No	Location	Feldspar	Pyroxene	Amphibole/ Pyroxene
421	44	SE¼,NW¼,Sec35 T27S, R4W	2	2	20
42A	44	SE¼,NW¼,Sec35 T27S, R4W	2	0	4
43	48	SE¼,Sec 35 T27S, R4W	0	0	0
44	55	NE¼,NE¼,Sec2 T27S, R4W	0	0	0
45	45	SE¼,SE¼,Sec26 T27S, R4W	8	0	2
46	76	S½, Sec 5 T29S, R3W	6	2	2
47	75	E½, Sec 8 T29S, R3W	6	0	0
48	73	NW¼, Sec 12 T29S, R4W	0	0	0
491	32	NW¼, Sec 2 T28S, R3W	0	2	4
492	32	NW¼, Sec 2 T28S, R3W	0	2	14
493	32	NW¼, Sec 2 T28S, R3W	2	2	10
50	31	NE¼, Sec 2 T28S, R3W	4	0	0
51	29	SW¼, Sec 26 T27S, R3W	0	4	0
521	30	NW¼, Sec 35 T27S, R3W	0	4	6
522	30	NW¼, Sec 35 T27S, R3W	4	0	0
53	33	NE¼, Sec 29 T27S, R3W	0	0	4

Sample No	Map No	Location	Feldspar	Pyroxene	Amphibole/ Pyroxene
531	33	NE¼, Sec 29 T29S, R3W	2	2	10
54	34	NW¼,NW¼,Sec28 T27S, R3W	30	6	20
551	42	N½, Sec 30 T27S, R3W	8	6	0
552	42	N½, Sec 30 T27S, R3W	6	8	2
56	46	NE¼, Sec 36 T27S, R4W	8	10	6
57	47	NW¼,SE¼,Sec36 T27S, R4W	12	0	4
58	54	SE¼,SE¼,Sec36 T27S, R4W	4	0	0
59	53	W½, Sec 6 T28S, R3W	6	2	18
60	51	W½, Sec 6 T28S, R3W	2	10	6
61	52	W½, Sec 6 T28S, R3W	2	4	16
62	17	E½, SE¼, Sec26 T26S, R3W	6	0	2
621	17	E½, SE¼, Sec26 T26S, R3W	40	8	2
63	16	SE½, SE¼, Sec6 T26S, R3W	34	2	8
64	15	N½,NE¼,Sec 7 T26S, R3W	30	4	8
65	12	NW¼,NE¼, T26S, R3W	4	0	18
66	4	SE¼, Sec 6 T26S, R3W	26	8	6

Sample No	Map No	Location	Feldspar	Pyroxene	Amphibole/ Pyroxene
67	18	NE¼,SE¼, T26S, R3W	30	0	0
68	2	NE¼,SE¼,Sec1 T26S, R4W	20	2	4
69	3	NW¼,SW¼,Sec 6 T26S, R3W	4	0	12
70	5	SW¼,SW¼,Sec 6 T26S, R3W	14	0	0
71	6	NW¼,NW¼,Sec 7 T26S, R3W	10	0	8
72	10	NW¼,NW¼,Sec 7 T26S, R3W	0	0	10
73	9	NW¼,NE¼,Sec12 T26S, R4W	8	0	0
74	8	SW¼,NE¼,Sec 1 T26S, R4W	18	0	2
75	7	NW¼,SE¼,Sec 1 T26S, R4W	46	0	0
751	7	NW¼,SE¼,Sec 1 T26S, R4W	38	0	2
76	1	SE¼,NE¼,Sec 1 T26S, R4W	8	2	2
89	78	N½,Sec 32 T28S, R3W	2	0	2
90	80	NW¼, Sec 28 T28S, R3W	3	1	4
96	77	S½,NE¼,Sec32 T28S, R3W	5	0	2
97	79	SE¼, Sec 20 T28S, R3W	1	2	0
			697	169	450

APPENDIX B

Description of Feldspar Megacrysts

Sample	Size (cm)	Weight (g)	Comments
13K	2X1½X1½	6.7	Clear to white megacryst with very finely-spaced twinning and shadows in fractured areas.
13L	3X2X1	6.9	Subrounded clear megacryst with coarse twinning.
54M	2½X1½X1	4.8	Clear megacryst with no visible twinning.
551A	2X1½X1	4.9	Subrounded megacryst with coarse twinning, carlsbad twinning and elongate strain shadows oriented at an approximate 40° angle from the twin plane.
56K	2X1½X1	5.0	White feldspar with red iron oxide stain, finely spaced twinning and carlsbad twinning.
57K	2X1X1½	6.0	Milky white megacryst with red iron oxide stain, finely spaced twins to coarse twins with minor pericline twinning where cracked and strained.
61K	2X1X1	5.0	Clear white megacryst with red iron oxide stain. Fine to coarse twinning with intense strain shadows and a microfault.
62A	3X2X1½	12.4	Subrounded, pitted megacryst with finely spaced twinning and showing moderate strain shadows.
621H	3½X2X1½	17.2	Clear to white megacryst with coarse to medium spaced twinning and minor ? apatite needles.
621I	3½X2X1	8.5	White to grey feldspar (two large crystals) with faulted twins and intense strain shadows.
621J	3X2X2	13.5	White megacryst with moderately spaced twinning and minor strain shadows.
621K	3½X2X1¼	9.2	Clear megacryst with finely-spaced twinning and ovoid pits filled with orange ? iron oxide.

90

Size (cm)	Weight (g)	Comments
3½X3X1	19.0	Subrounded pitted megacryst with finely spaced albite and pericline twinning.
2½X2X1	10.0	Clear to white megacryst with moderately spaced twinning.
3X2X1	8.6	Clear to white megacryst with fine to coarsely spaced twinning and several elongate open pits.
3X1½X1½	6.3	Clear, dull megacryst with fine to coarsely spaced twinning.
3X2X½	3.6	Clear megacryst with no visible twinning.
3X1½X1	10.7	White megacryst with red iron oxide staining. No visible twinning and faint strain shadows.
3X2½X2	23.3	Subrounded megacryst, extremely pitted grey-white megacryst with red iron oxide stain. Finely spaced twinning and intense strain shadows. Twins seem almost bent. Pits are void or filled with iron oxide.
2½X1X1	5.0	White megacryst with fine to moderately spaced twins and carlsbad twins.
3X2X1	9.9	Clear to white megacryst with very coarsely spaced twins and parallel elongate void pits.
2X1X1	2.9	White megacryst with no visible twinning.
3X1X1	4.8	Clear, pitted and fractured megacryst with no visible twinning and slight strain shadows.
3X2X1	5.8	White megacryst with coarsely spaced twinning.
3X2X1½	15.0	Clear to white megacryst with coarsely spaced twinning.
2X1½X1	4.3	Grey megacryst with finely spaced twinning and intense strain shadows.
2X2X½	3.2	Clear megacryst with no visible twinning.

APPENDIX C

ESTIMATED COMPOSITION OF MAFIC AND ULTRAMAFIC

SAMPLES IN VOLUME PERCENT (±5%)

SAMPLE	PLAG	CLPX	AMPH	OL	PEROV-SKITE/SPINEL	GLASS	OTHER
13B-4			95		5		
13G-S		25	60	3	15		
13G-U		70	8		21		1-1euc
13H		75	5	10	7	3	
13I		89	5	1	5		
141P	5	30	40	5	20		
21B		40	40	10	12		
222A		92	3		5		
221C	5	30	5	55		5	
222B					100		
27A		92	3		5		
27C	5	70		5	10	10	
27E		85			10	5	
27J		80	10		14		
294H		60		15			10opx15bas
319		60	15	15	12		
34B		85			15		
382A	25	25			50		
40E-S		60			40		
40E-U		10		70	5		15 idd
40-H		60		20			5opx15bas
40N		2		65	10	20	
42B		60		15	5	10	15idd
42D		60		20	15	10	
42EX-1	5	50		30	5		10bas
42EX-2		70			20	10	
42EX-3		60		15	10	20	
421N		35	60		2		5mica

APPENDIX C

Continued

SAMPLE	PLAG	CLPX	AMPH	OL	PEROV/ SPINEL	GLASS	OTHER
421-0	5	35	35	10	7		10 mica
421P	5	10	75		10		
492A		80			20		
492D		45			55		
93H		65			5	15	
53B		65			10		25bas
53I		85	5	2	5		3idd
531A		25	5	60	10	5	
54A	5	80			10	5	
54C		70			30		
551C		65		10	15		10bas
552J		70			10	20	
56A		100					
56G			85				15bas
56I			90		3		7bas
59C		70	10	5	5	10	
59D		70	15	5	5	5	
60A	5	20	75				
60B		10	75		10		5 mica
60C	5	80	15				
60F	5	55	20		15	5	
60I		65	10		20	5	
61B		60	10	10	20		
61C		25	30	25	15		
61D		25	30	20	20	5	
621F	15	25	50		10		
63P			90				10bas
63R	15	10	70		5		
64A	60	10	30				

APPENDIX C

Continued

SAMPLE	PLAG	CLPX	AMPH	OL	PEROV/ SPINEL	GLASS	OTHER
64S	7	50	30	10	3		
65A	10	10	80				
65B	5	20	70		15		
68C		50	35		5		
69J		50	35	5	5		5idd
71D		80	5		15		
72B		60		20			20idd
382	80						20K-spar

leuc = leucoxene

opx = orthopyroxene

bas = basalt

idd = iddingsite